AI-66-21

SUMMARY REPORT

INVESTIGATION OF CURRENT DEGRADATION PHENOMENON IN SUPERCONDUCTING SOLENOIDS

JANUARY 14, 1966

Contract NAS8-5356

MARSHALL SPACE FLIGHT CENTER

Huntsville, Alabama

AI-66-21

SUMMARY REPORT

INVESTIGATION OF CURRENT DEGRADATION PHENOMENON IN SUPERCONDUCTING SOLENOIDS

JANUARY 14, 1966

ATOMICS INTERNATIONAL
A Division of North American Aviation, Inc.
Box 309, Canoga Park, California

Contract NAS8-5356

MARSHALL SPACE FLIGHT CENTER

Huntsville, Alabama

CONTENTS

TABLES

FIGURES

FIGURES

FIGURES

ABSTRACT

This report covers work performed through January 14, 1966 under NASA Contract NAS8-5356. A total of 30 samples of Ti - 22 at. % Nb, representing 30 separate variations of aging time and temperature, were fabricated and tested to determine the effect of metallurgical preparation on the superconducting properties of such transition-metal alloy superconductors. A maximum was found for critical current density with respect to aging temperature; a broader maximum as a function of aging time. None of the samples tested exhibited any super-current instabilities for values of dH/dt up to the maximum rate of 2000 Gauss/sec while the field was in the positive sense; SN transitions were observed for 3 samples as the field sense became negative for values of dH/dt > 1000 Gauss/sec.

Broad double transitions were observed for both H_r and T_c (initial temperature) samples aged at 600 to 650°C. Correlations between the metallurgical and physical properties indicate that H_r and T_c of warm-aged Ti - 22 at. % Nb are functions of the composition of the continuous phase of the alloy. Also, the flux pinning effect of the α-Ti precipitate has been correlated with precipitate spacing. The results thus indicate that the superconducting properties of Ti - 22 at. % Nb pertinent to magnet design can be varied in a predictable manner. It is also felt that the method described for optimizing the high superconducting properties is applicable to most of the binary transition-metal alloy systems.

Mr. L. C. Salter was the principal investigator; Mr. J. Raymond prepared the 30 samples and conducted the critical current survey. Dr. R. W. Boom and Mr. J. B. Vetrano made various advisory contributions to the work. High field facilities were made available at the North American Science Center and at Oak Ridge National Laboratory.*

*We particularly thank Drs. T. G. Berlincourt and A. C. Thorsen of the NAA Science Center for the use of their pulsed magnets and Dr. W. F. Gauster, ORNL, for the use of a large bore dc field facility.

I. Ti–Nb CHARACTERIZATION

A. INTRODUCTION

It has been shown that bulk superconducting properties, such as upper critical field (H_{c2}) and critical temperature (T_c), of homogeneous, transition-metal alloys are determined by the metallurgical composition of the superconductor.[1, 2] It is also known that the critical current (J_c) of Type II alloy superconductors is greatly dependent upon metallurgical microstructure, although the mechanism is only qualitatively understood. Thus, high field superconducting properties, in particular J_c, T_c, and H_{c2}, are determined by metallurgical composition and microstructure, and the high field characteristics can be varied by proper metallurgical preparation.[2] It is the purpose of this portion of the program to investigate the effect of metallurgical preparation on the superconducting properties of such transition-metal alloy superconductors. The approach taken was to study a single binary alloy; the Ti - 22 at. % Nb alloy was chosen because company-sponsored research has revealed that J_c of this alloy can be greatly improved with simple warm aging treatments (see Figure 1) without requiring severe cold work.[2] To completely explore the effect of heat treatment on this alloy, combinations of warm aging time and temperature were chosen according to the schedule in Figure 2. The temperature range in the warm-aging schedule was chosen to span the two-phase region of the Ti-Nb phase diagram,[3] shown in Figure 3. From this diagram, it is seen that at equilibrium a two-phase structure (α-Ti and β-Nb) will result at temperatures less than 680°C.

The tests performed on each sample were:

1) Metallurgical tests: photomicrographs, KHN hardness, and x-ray diffraction patterns for composition determinations.

2) Superconducting tests: resistive upper critical field ($H_r \simeq H_{c2}$), critical temperature (T_c), and critical current (J_c) versus applied transverse field.

3) Other measurements included normal state resistivity at 300°K and 4.2°K.

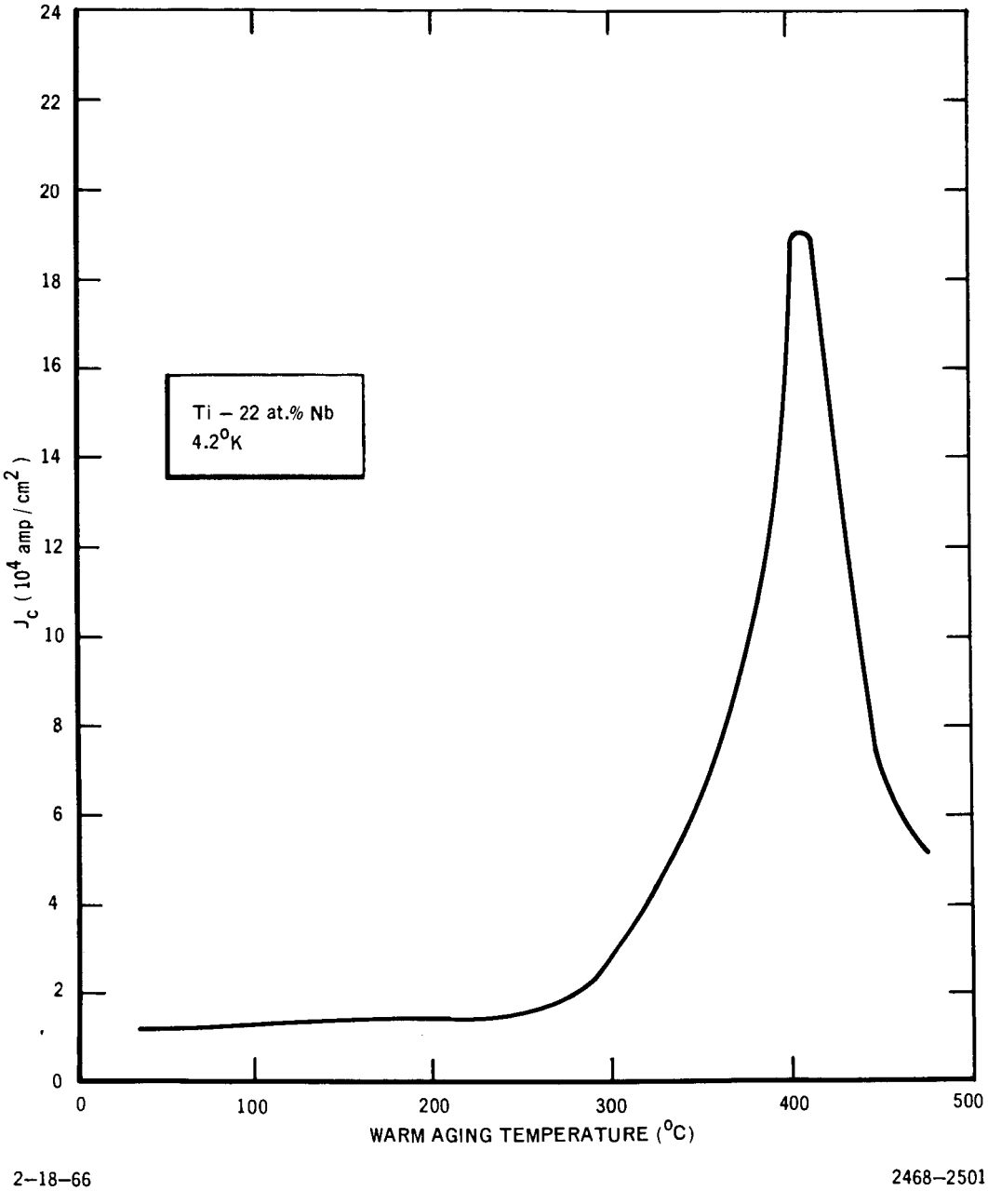

Figure 1. Critical Current Density of Ti - 22 at. % Nb vs Warm Aging Temperature

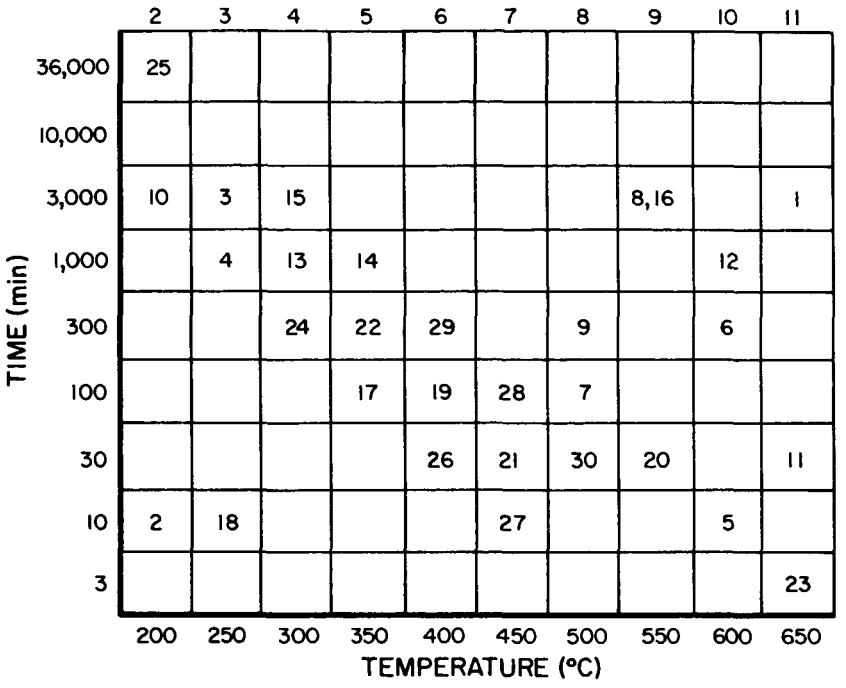

2-18-66 00-153158A

Figure 2. Warm Aging Schedules for Ti - 22 at. % Nb Wire Samples (Sample numbers are shown in squares)

The sample form chosen was a 0.010-in. -diameter wire. Samples were prepared, then heat treatments were completed according to the schedule shown in Figure 2. Two 4-in. -long samples were annealed at each time and temperature: one sample for metallurgical examinations, H_r and T_c tests and one for J_c versus transverse H tests. The latter sample was bent into hairpin shape before annealing. The tests, results, and correlations are presented below.

B. CRITICAL CURRENT MEASUREMENTS

1. Experiment

The critical current density versus transverse magnetic field curves (J_c versus H) were measured on warm aged samples mounted in hairpin fashion. Super-to-normal joints were made by inserting the chemically cleaned wire ends in a 0.025-in. -diameter by 1.0-in. hole drilled in well-annealed 0.10-in. -diameter copper conductor and pressing the joint in a common laboratory press.

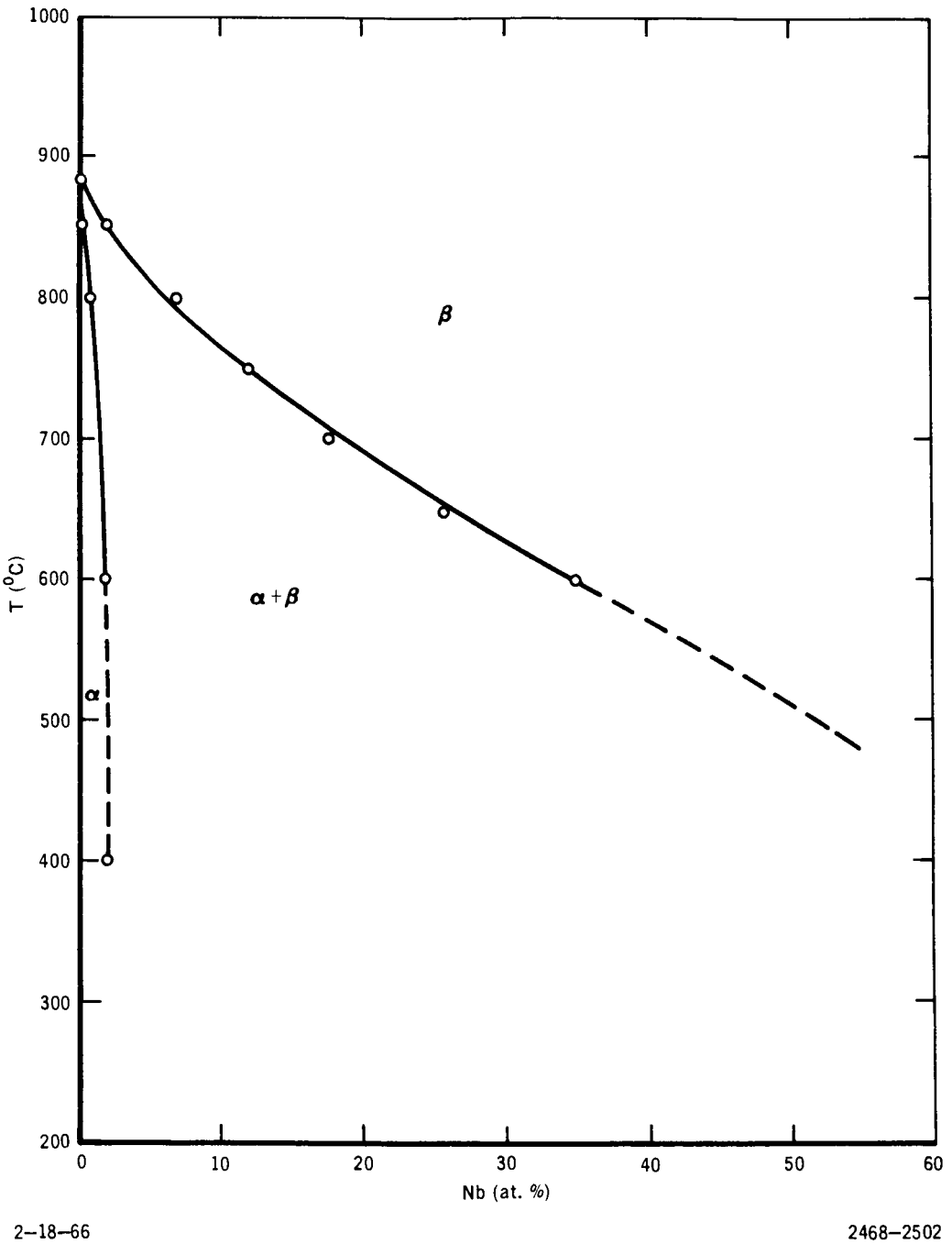

Figure 3. Ti-Nb Phase Diagram

The sample and joints were then secured by potting in Emerson and Cumings Stycast No. 2850 FT epoxy. The J versus H measurements were taken at 4.2°K in fields up to 45 kgauss (supplied by a superconducting solenoid). Sample current was supplied by a 12-volt battery bank and controlled with two large carbon-pile resistors. The experimental circuitry is shown in Figure 4.

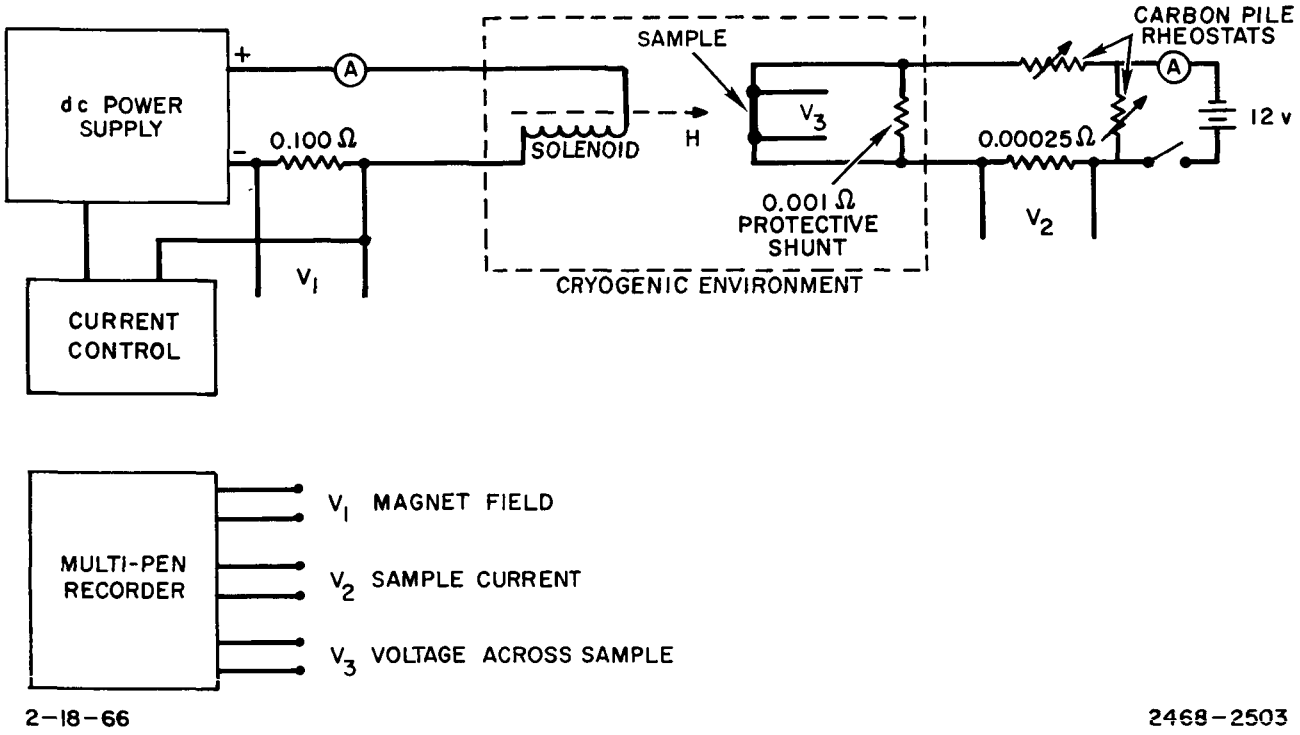

Figure 4. Experimental Circuitry for Short Sample J versus H and Stability Tests

The experimental procedure consisted of holding the field constant and increasing sample current until the wire went normal. This procedure defined a unique curve which was labeled the standard J versus H curve. All tests were repeated after a 6-month interval to eliminate the possibility of room-temperature aging; none was observed.

2. Results

The J_c versus H curves are shown in Figures 5 through 15, in conjunction with the upper critical field measurements. Critical field measurements are discussed in Section I.D. Each figure shows results for wire samples annealed at the same temperature for different times. Values for J_c at 20 kG as a function of warm-aging time and temperature are listed in Table 1. It reaches a well-defined maximum for ~400°C aging temperature, and a broad maximum in the aging time between 300 and 1000 min.

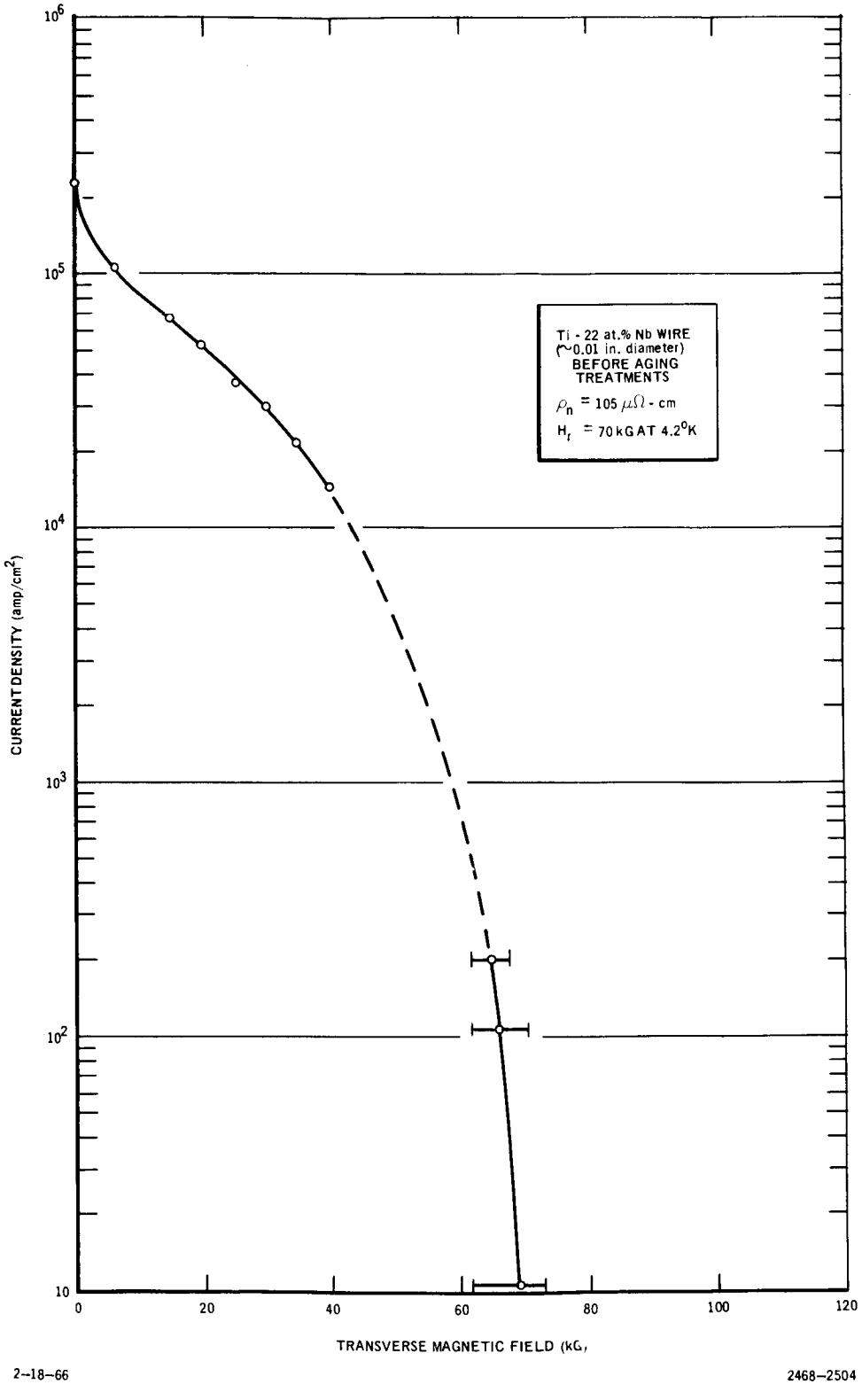

Figure 5. Critical Current Density and Upper Critical Field at 4.2°K for 0.01-in.-Diameter Ti - 22 at. % Nb Wire, β-Quenched From 800°C at 0.016 in. Diameter and Drawn to 0.01 in. Diameter

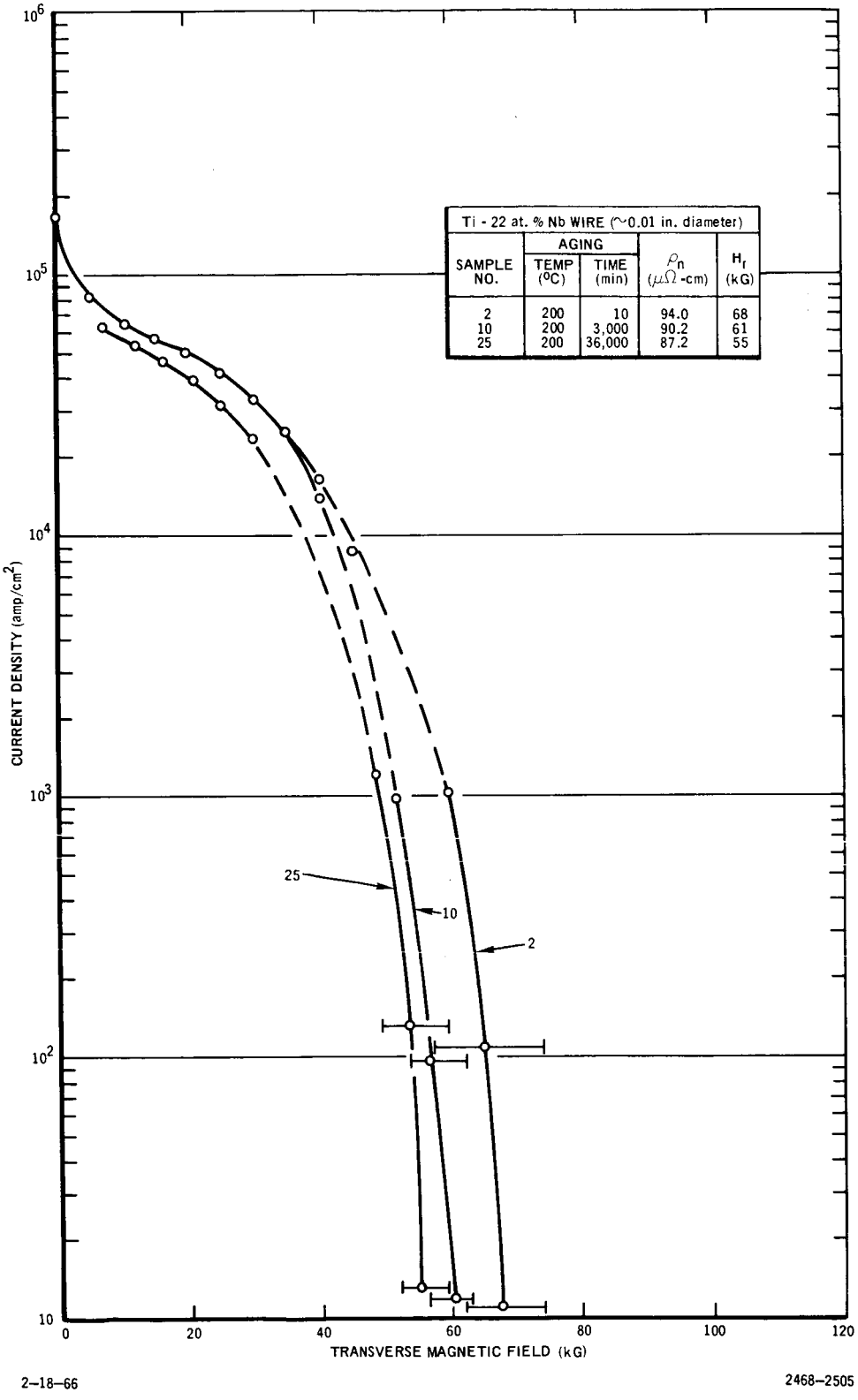

Figure 6. Critical Current Densities and Resistive Upper Critical Fields at 4.2°K for 0.01-in. - Diameter Ti - 22 at. % Nb Wires Warm Aged at 200°C for the Times Shown

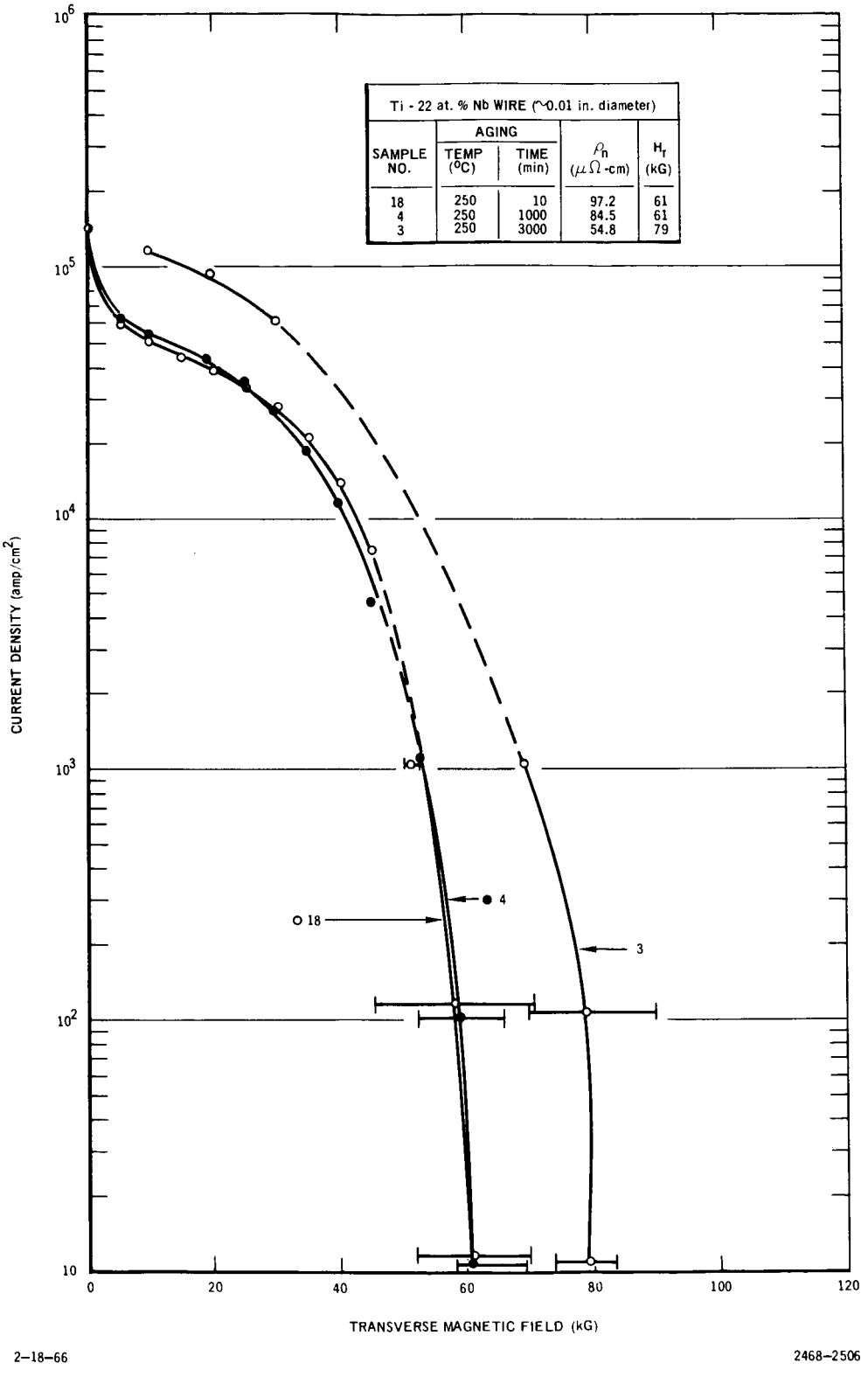

Figure 7. Critical Current Densities and Resistive Upper Critical Fields at 4.2°K for 0.01-in. - Diameter Ti - 22 at. % Nb Wires Warm Aged at 250°C for the Times Shown

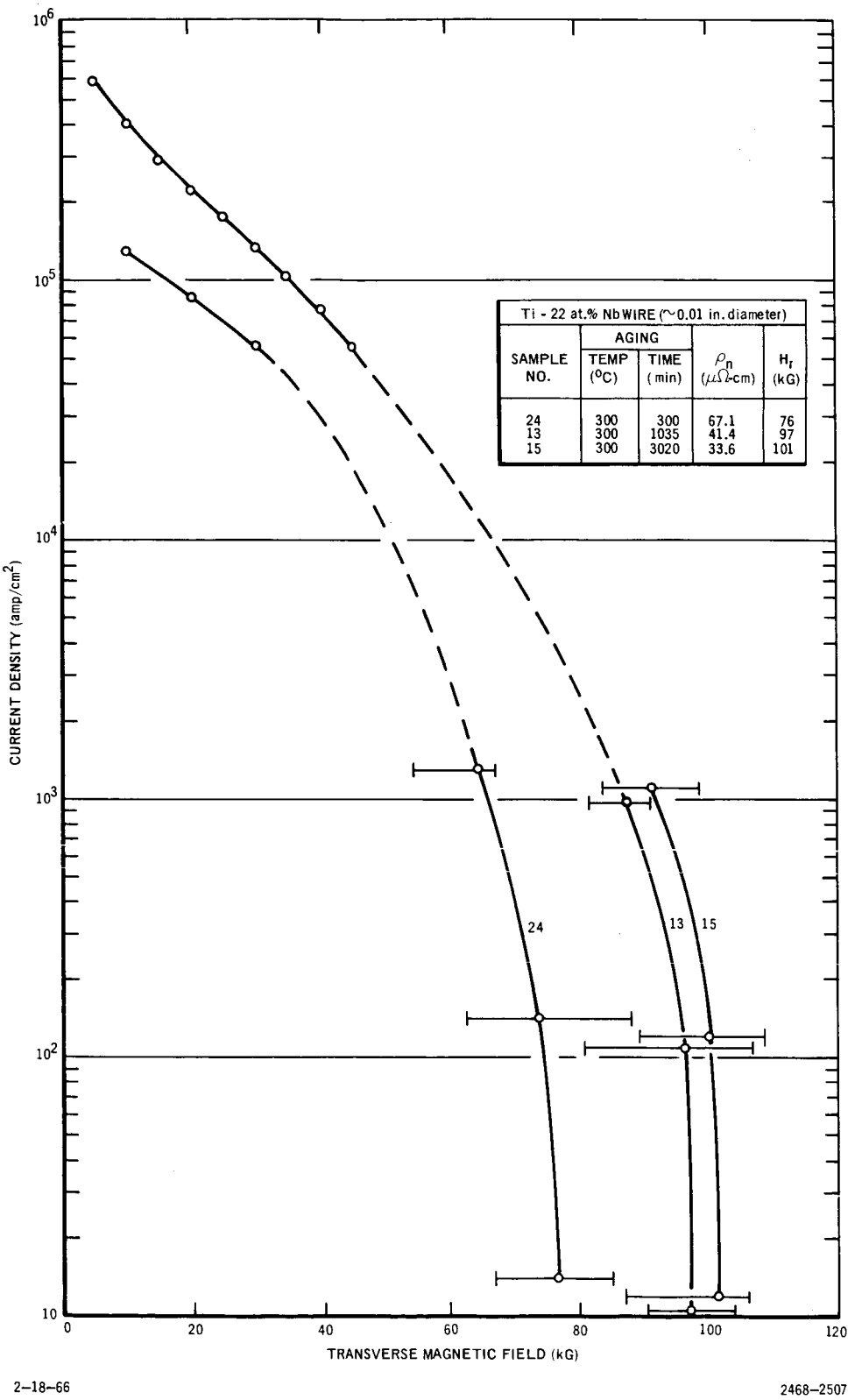

Figure 8. Critical Current Densities and Resistive Upper Critical Fields at 4.2°K for 0.01-in. - Diameter Ti - 22 at. % Nb Wires Warm Aged at 300°C for the Times Shown

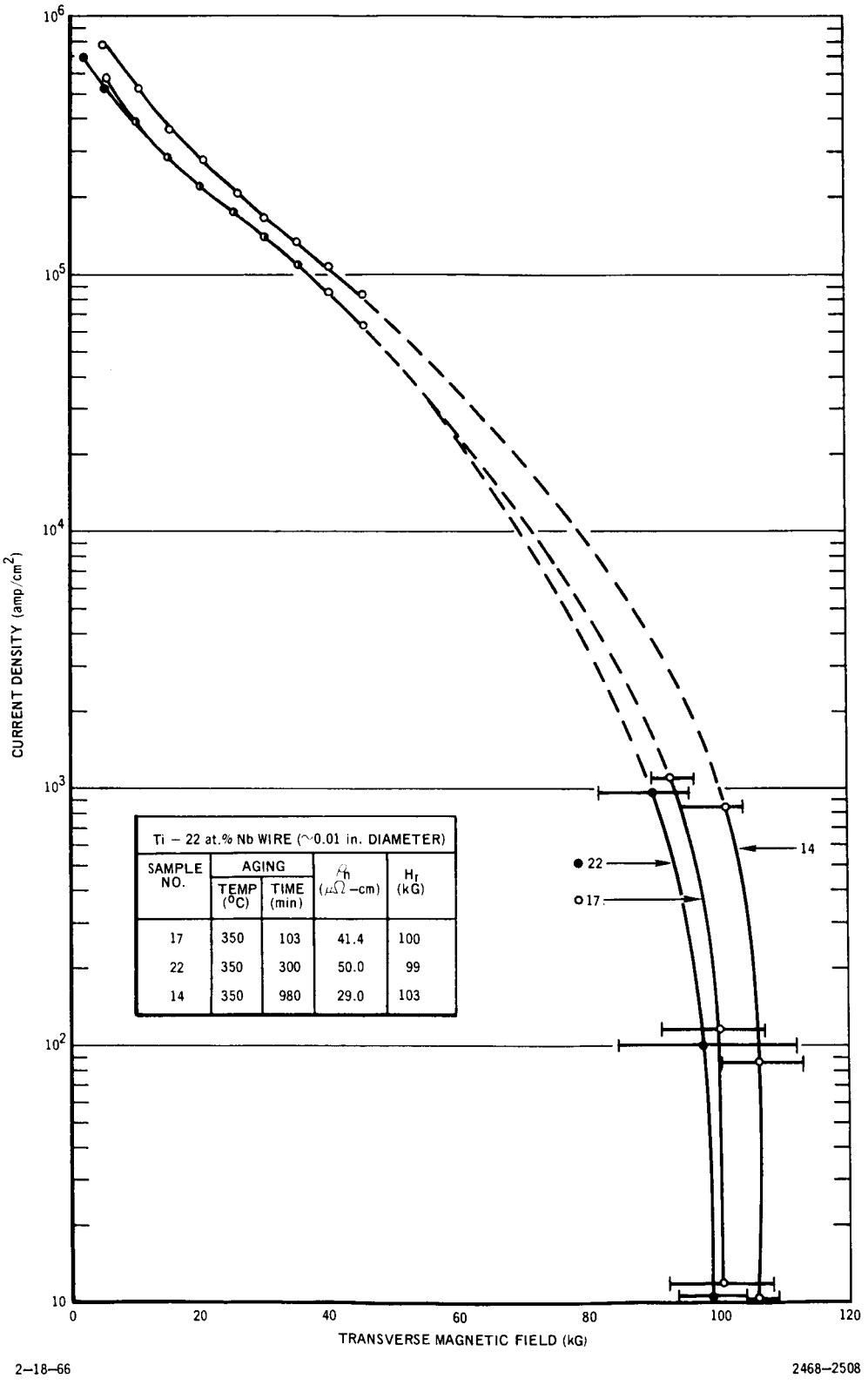

Figure 9. Critical Current Densities and Resistive Upper Critical Fields at 4.2°K for 0.01-in. - Diameter Ti - 22 at. % Nb Wires Warm Aged at 350°C for the Times Shown

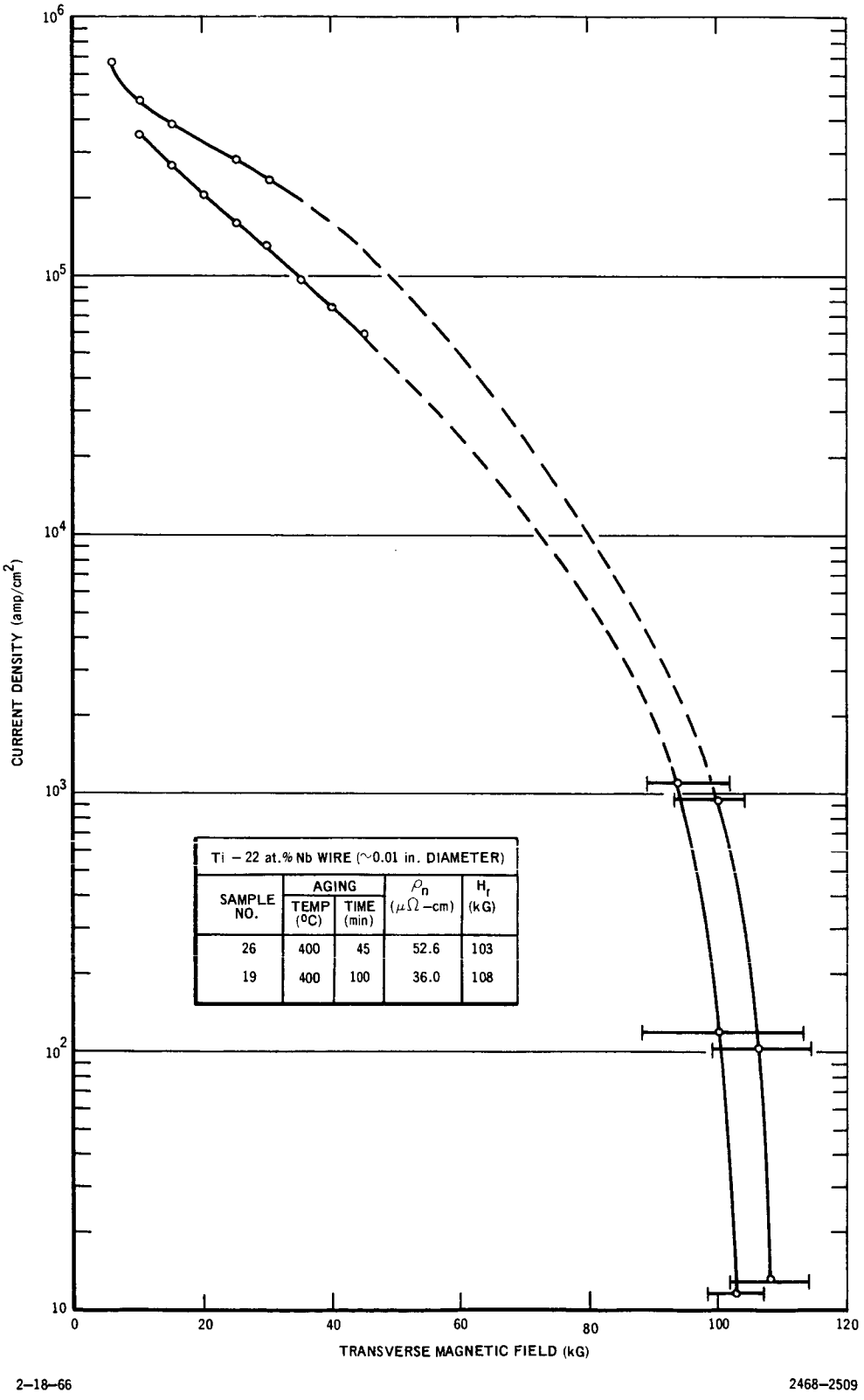

Figure 10. Critical Current Densities and Resistive Upper Critical Fields at 4.2°K for 0.01-in. - Diameter Ti - 22 at. % Nb Wires Warm Aged at 400°C for the Times Shown

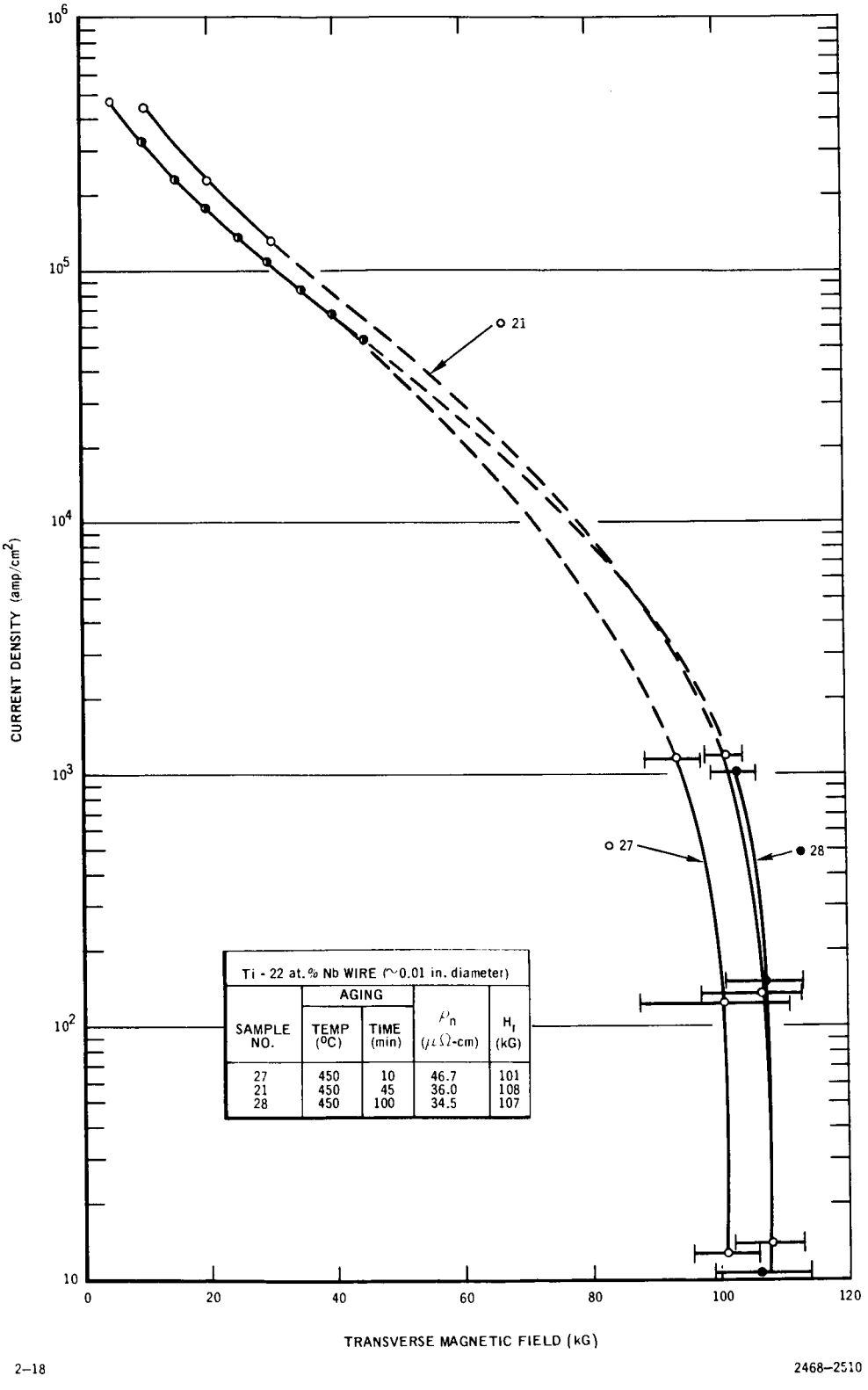

Figure 11. Critical Current Densities and Resistive Upper Critical Fields at 4.2°K for 0.01-in.-Diameter Ti - 22 at.% Nb Wires Warm Aged at 450°C for the Times Shown

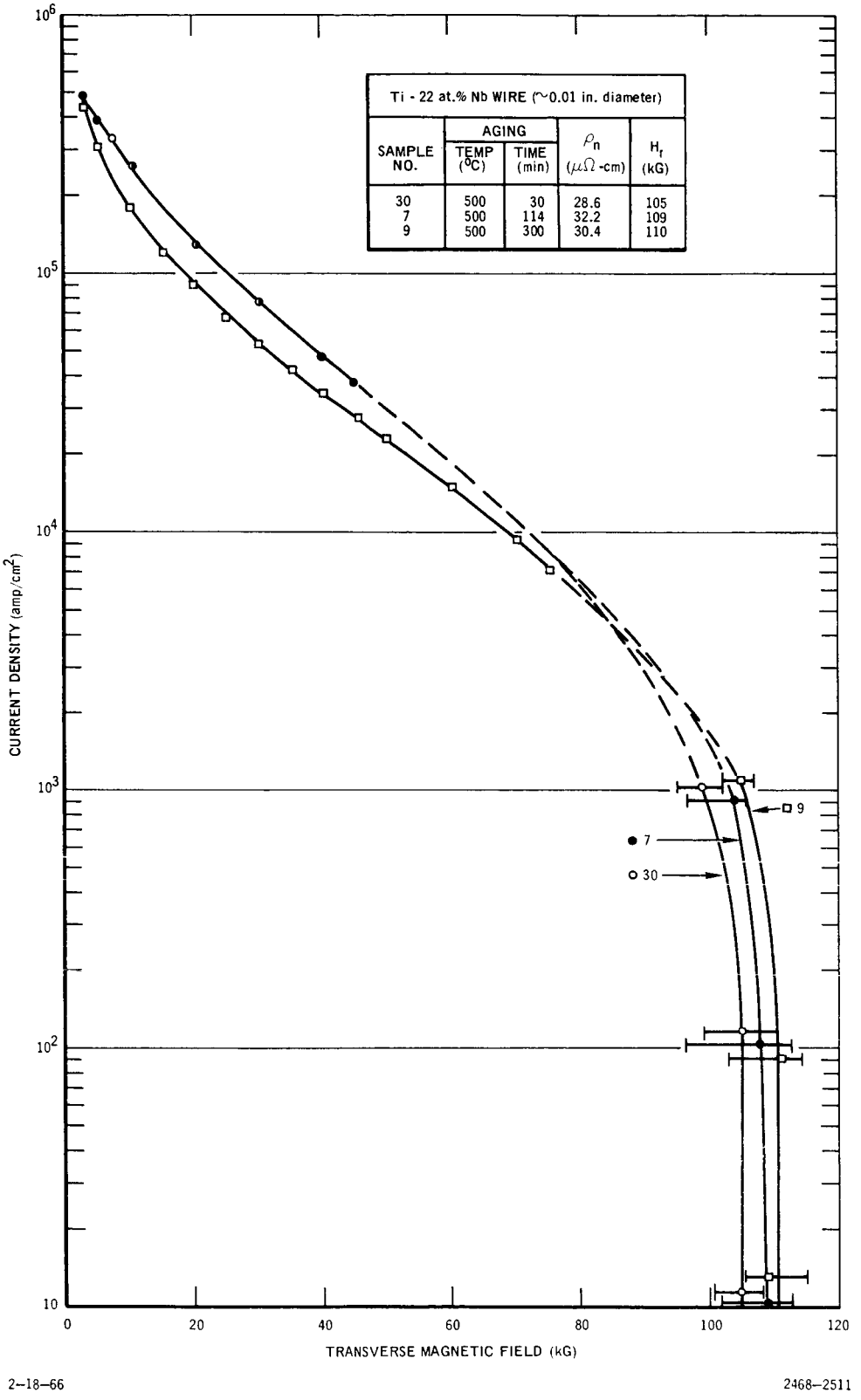

Figure 12. Critical Current Densities and Resistive Upper Critical Fields at 4.2°K for 0.01-in. - Diameter Ti - 22 at. % Nb Wires Warm Aged at 500°C for the Times Shown

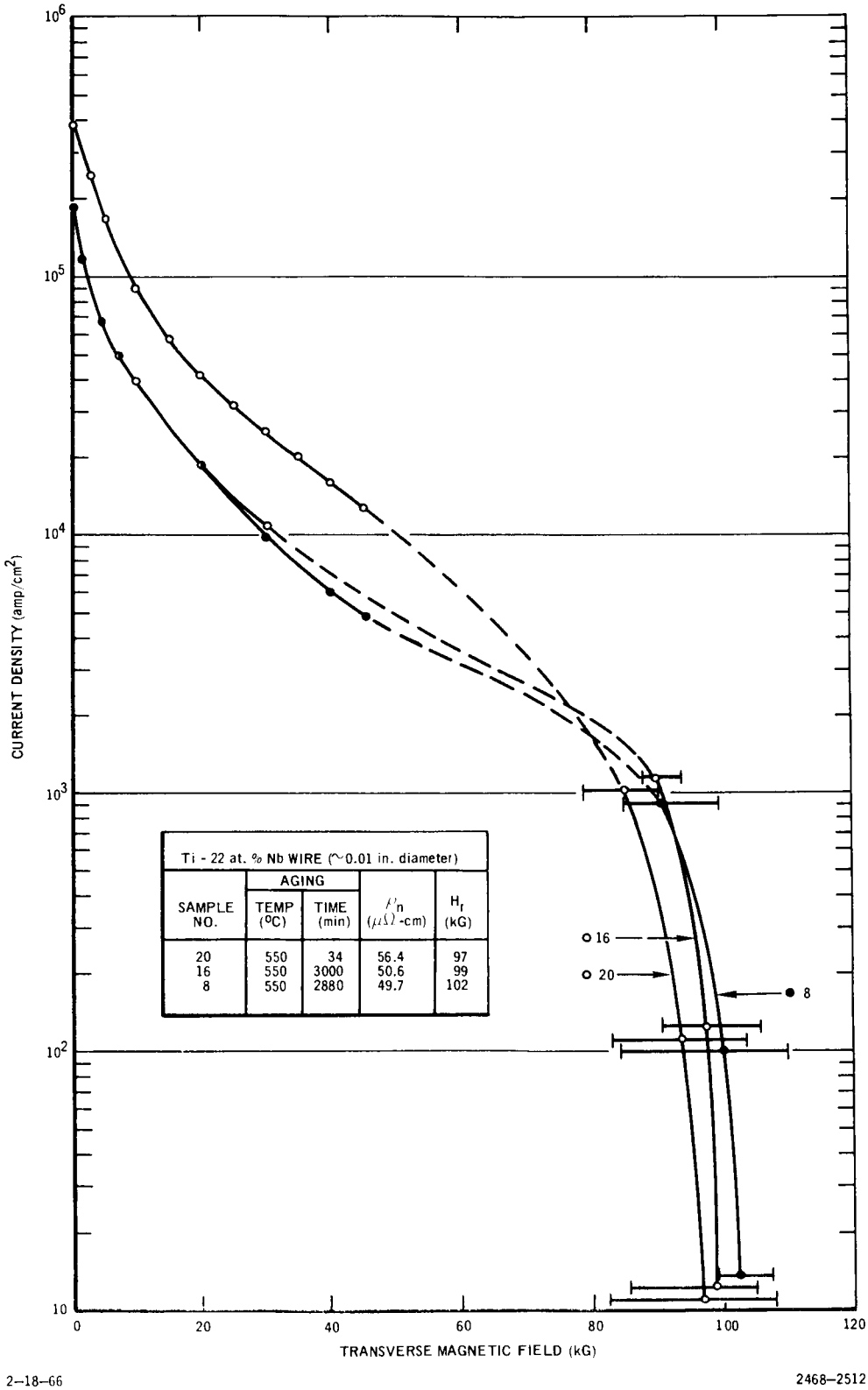

Figure 13. Critical Current Densities and Resistive Upper Critical Fields at 4.2°K for 0.01-in. - Diameter Ti - 22 at. % Nb Wires Warm Aged at 550°C for the Times Shown

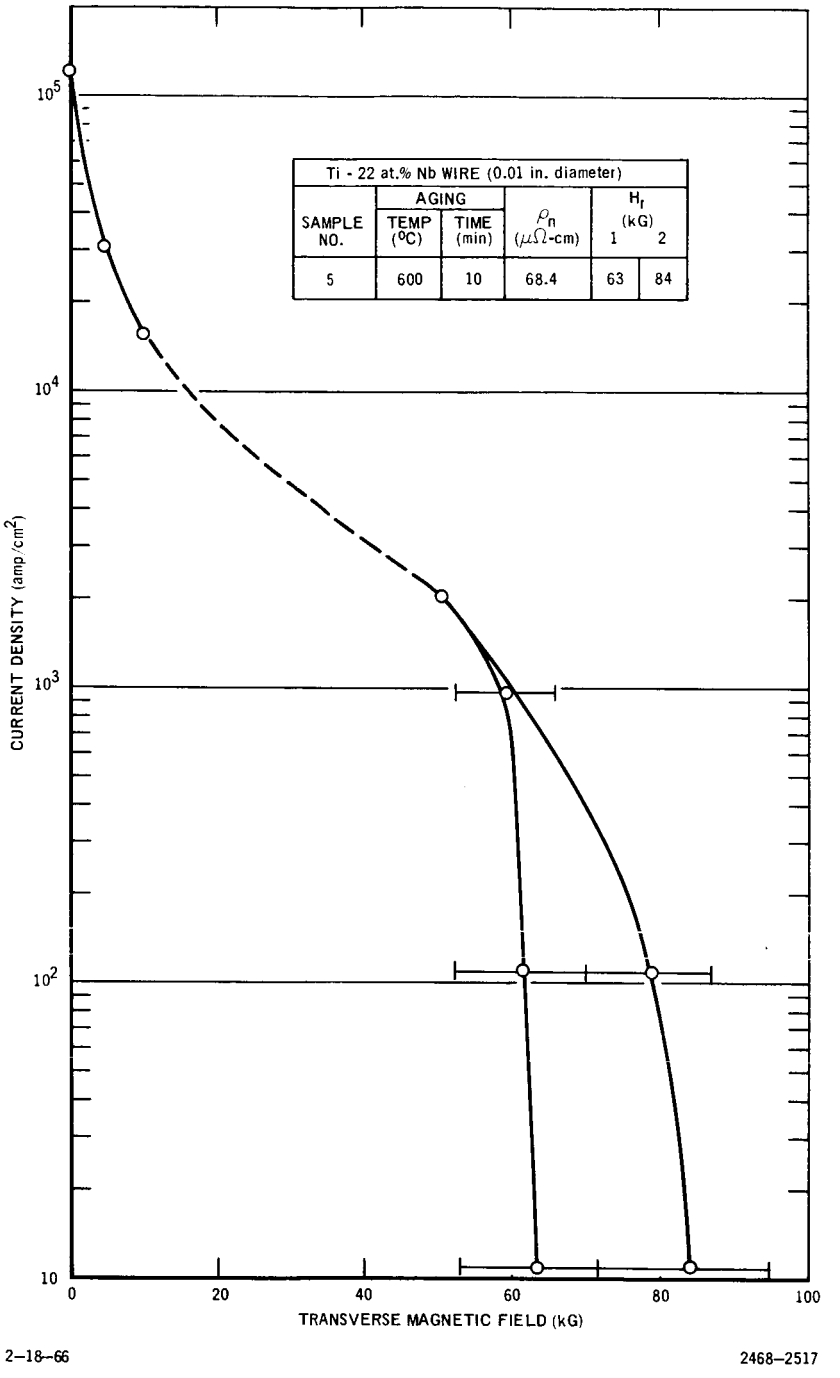

Figure 14a. Critical Current Densities and Resistive Upper Critical Fields at 4.2°K for 0.01-in.-Diameter Ti - 22 at. % Nb Wires Warm Aged at 600°C for the Times Shown, Sample 5

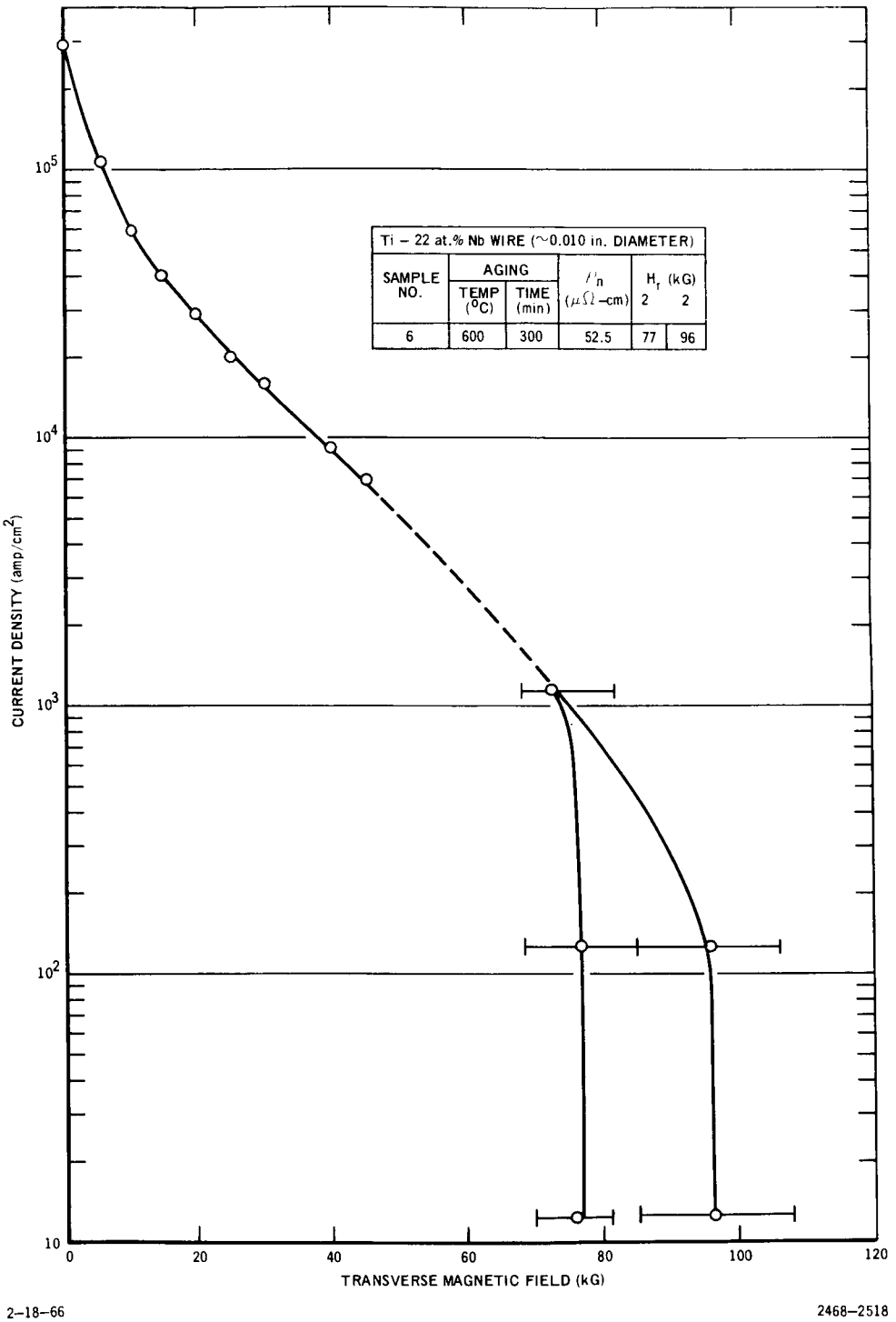

Figure 14b. Critical Current Densities and Resistive Upper Critical Fields at 4.2°K for 0.01-in.-Diameter Ti - 22 at. % Nb Wires Warm Aged at 600°C for the Times Shown, Sample 6

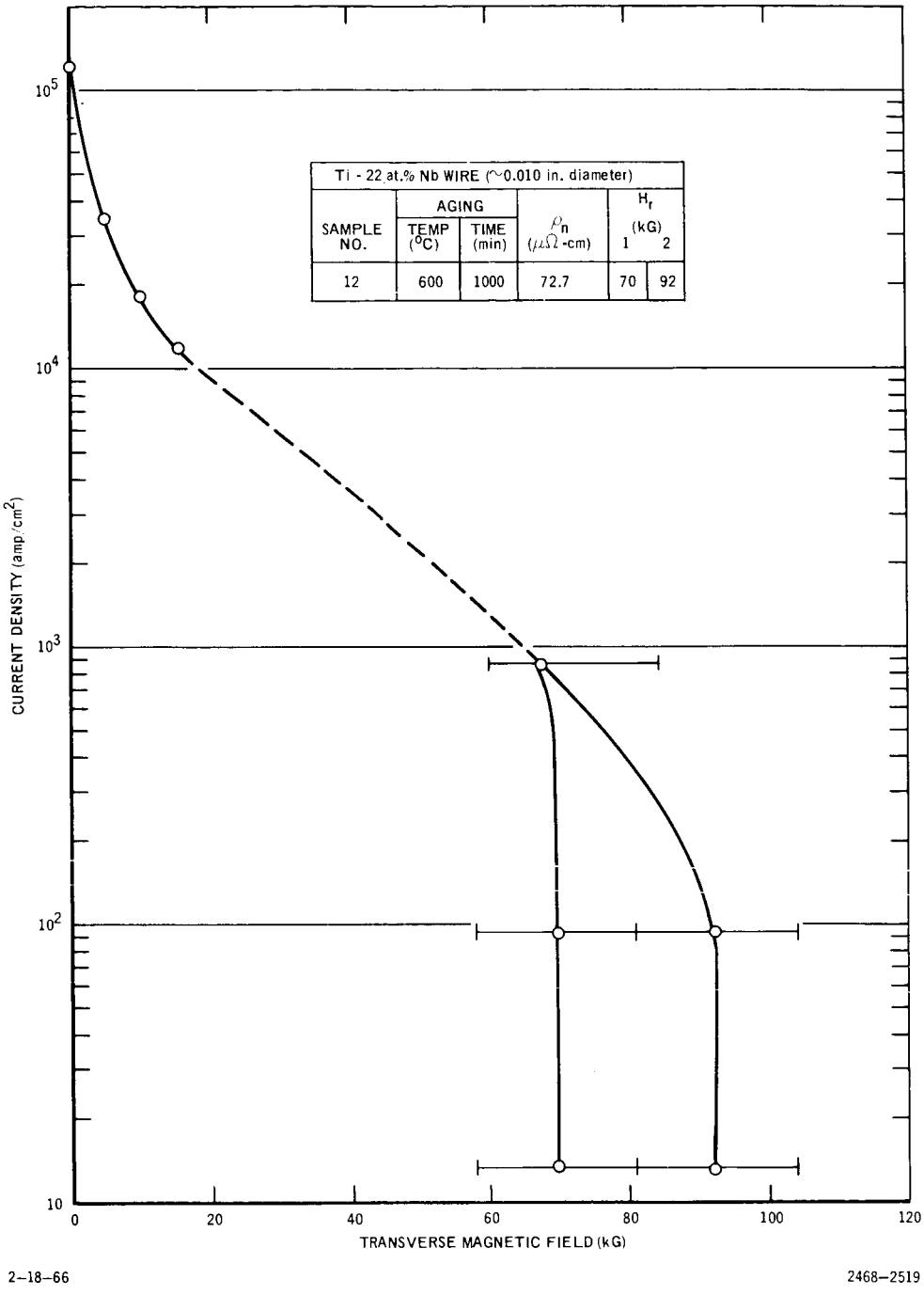

Figure 14c. Critical Current Densities and Resistive Upper Critical Fields at 4.2°K for 0.01-in. - Diameter Ti - 22 at. % Nb Wires Warm Aged at 600°C for the Times Shown, Sample 12

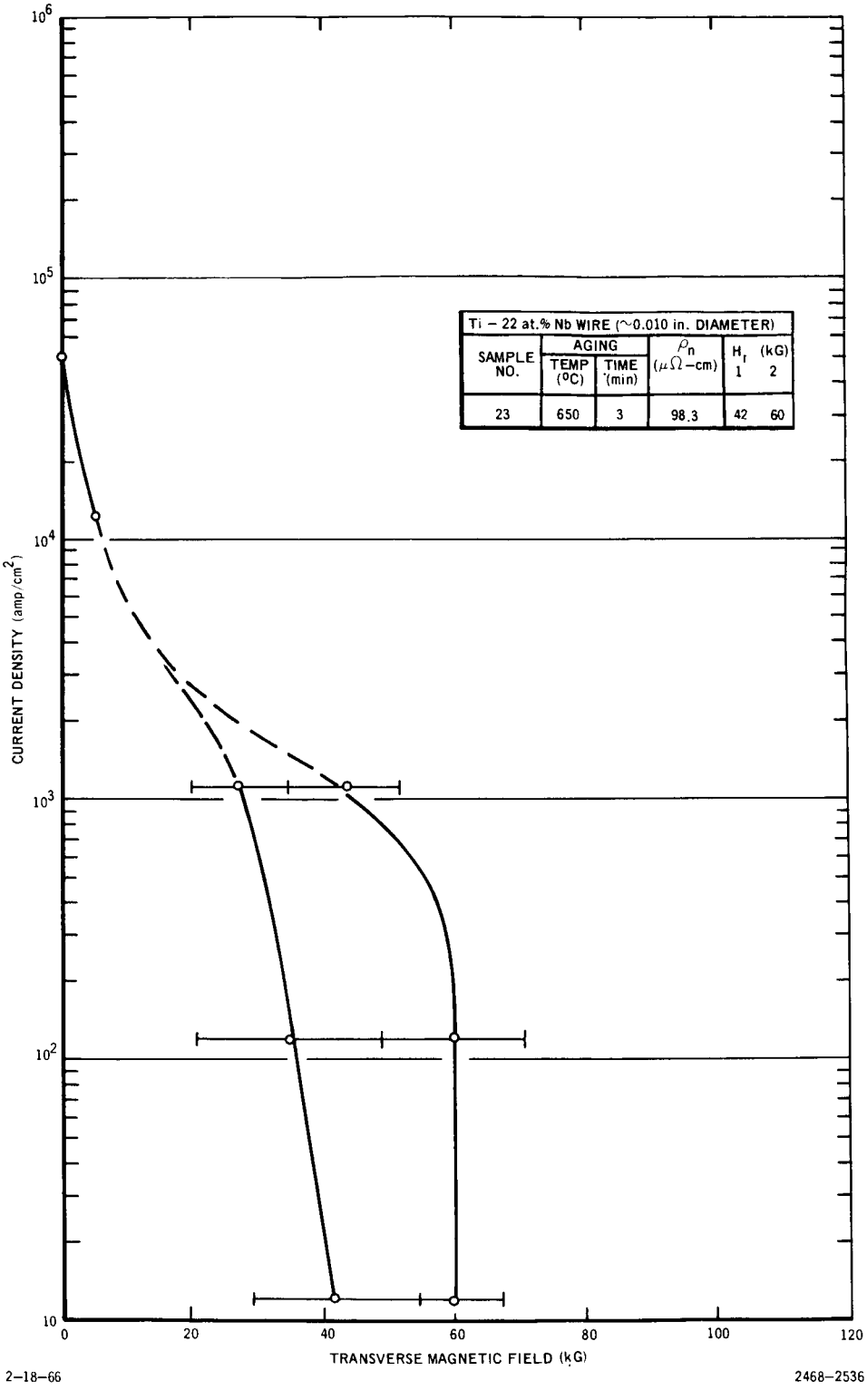

Figure 15a. Critical Current Densities and Resistive Upper Critical Fields at 4.2°K for 0.01-in. - Diameter Ti - 22 at. % Nb Wires Warm Aged at 650°C for the Times Shown, Sample 23

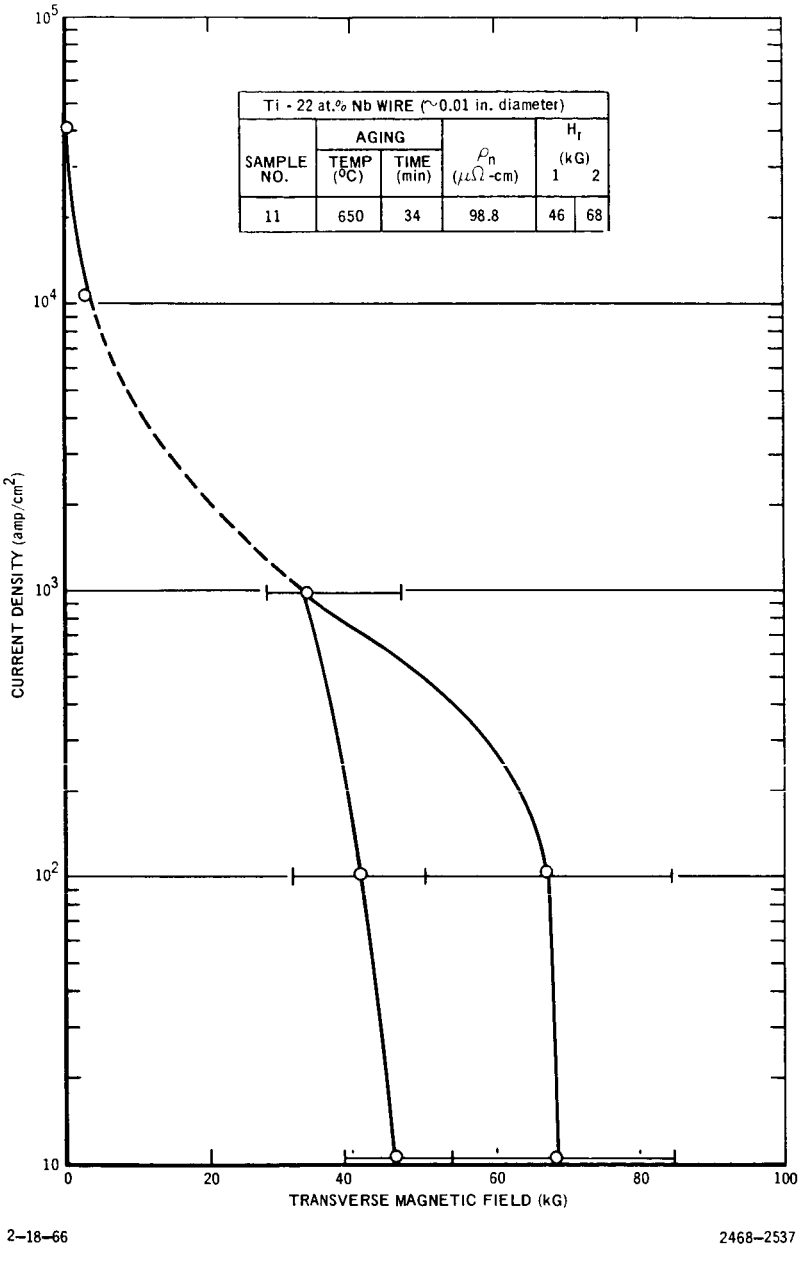

Figure 15b. Critical Current Densities and Resistive Upper Critical Fields at 4.2°K for 0.01-in.-Diameter Ti - 22 at. % Nb Wires Warm Aged at 650°C for the Times Shown, Sample 11

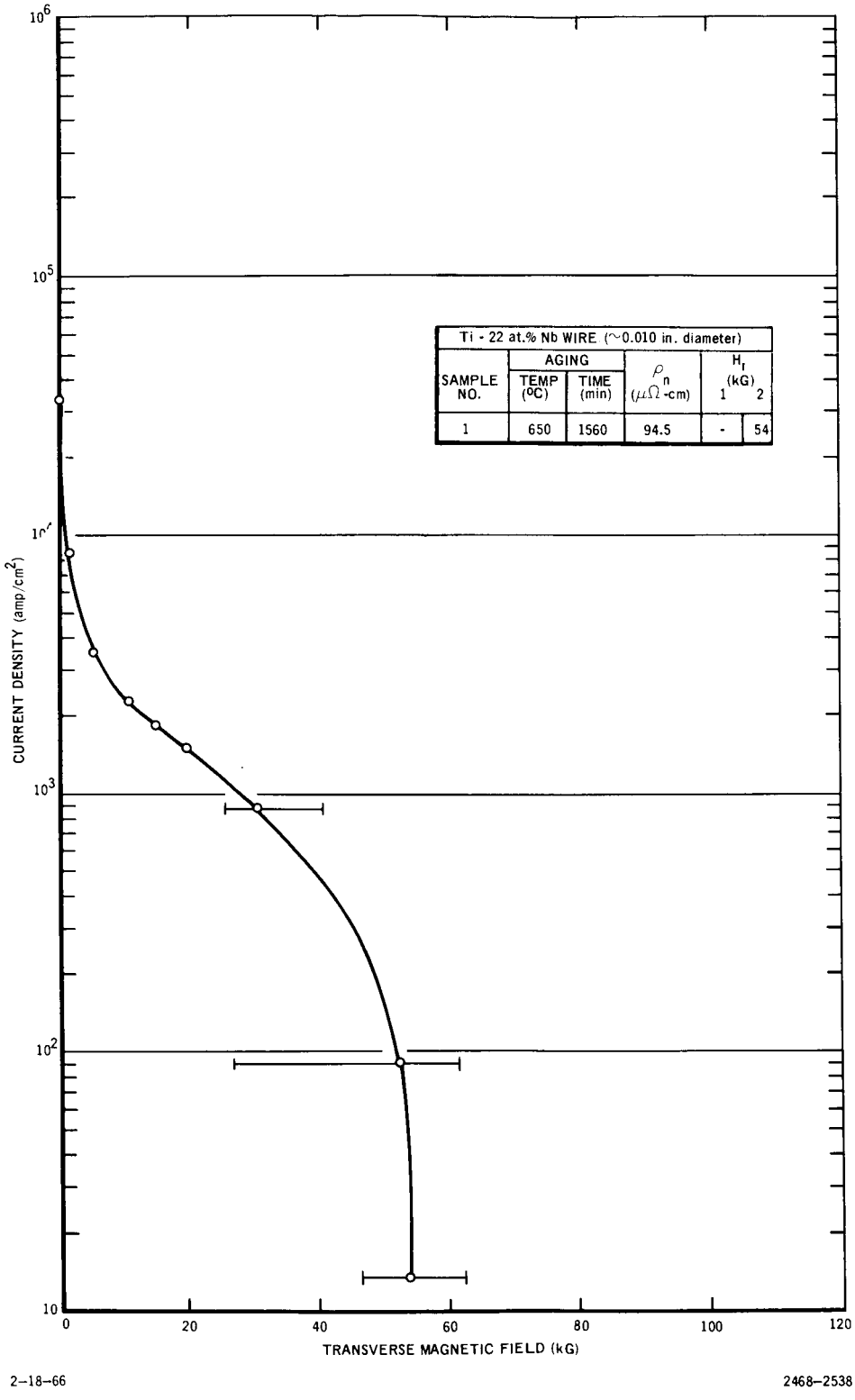

Figure 15c. Critical Current Densities and Resistive Upper Critical Fields at 4.2°K for 0.01-in. - Diameter Ti - 22 at. % Nb Wires Warm Aged at 650°C for the Times Shown, Sample 1

TABLE 1

SUMMARY OF MEASURED PHYSICAL PROPERTIES OF
Ti - 22 at. % Nb ALLOY AFTER VARIOUS WARM AGING TREATMENTS

Aging Parameters		Sample	Post-aging Resistivity at 300°K ρ_f ($\mu\Omega$-cm)	Normal State Resistivity at 4.2°K ρ_n ($\mu\Omega$-cm)	Hardness (KHN)	J_c at 20 kG (10^4 amp/cm^2)	T_c* (°K)	H_r* at 4.2°K (kG)	Nb in β-Phase (at. %)
Temperature (°C)	Time (min)								
		800°C	115 ±2	105	282	5.0	6.98	70	22.0
200	10	2	107	94	241	5.0	6.93	68	22.0
	3000	10	107	90	395	5.2	6.49	61	22.0
	36,000	25	NA†	87	NA	4.0	6.47	55	22.0
250	10	18	103	97	382	4.0	6.78	61	22.0
	1000	4	105	84	426	4.2	6.51	61	22.0
	3000	3	88	55	480	16.0	7.55	79	23.4
300	300	24	81	67	NA	8.6	7.20	76	~23.0
	1035	13	82	41	423	22.0	8.50	97	40.8
	3020	15	69	34	207	NA	8.70	101	47.5
350	103	17	75	41	423	22.0	8.38	100	44.2
	300	22	59	50	454	23.0	8.48	99	46.0
	980	14	68	29	409	26.0	8.89	106	46.7
400	45	26	78	53	370	21.0	8.26	103	44.9
	100	19	71	36	423	31.5	8.67	108	43.1
	300	29	67	NA	360	NA	NA	NA	NA
450	10	27	79	47	359	17.5	8.18	101	44.2
	45	21	66	36	NA	23.5	8.61	108	41.7
	100	28	71	34	347	16.5	8.75	107	53.6
500	30	30	68	29	NA	13.0	8.51	105	44.9
	114	7	72	32	211	11.5	8.60	109	42.6
	300	9	71	30	282	8.9	8.81	110	48.9
550	34	20	77	56	253	4.1	8.16	97	40.8
	3000	16	75	51	NA	1.9	8.32	99	41.2
	2880	8	77	50	207	1.8	8.51	102	37.3
600	10	5	85	68	226	0.85	7.53	84	32.9
							7.33	63	
	300	6	88	52	236	2.80	8.19	96	39.6
							7.92	76	
	1000	12	90	73	NA	0.91	8.03	92	35.7
							NA	70	
650	3	23	70	98	NA	0.19	6.79	60	~23
							6.38	42	
	34	11	113	99	234	0.23	6.89	68	23.4
							6.66	46	
	1560	1	108	94	216	0.16	6.70	54	25.7

†Not applicable.

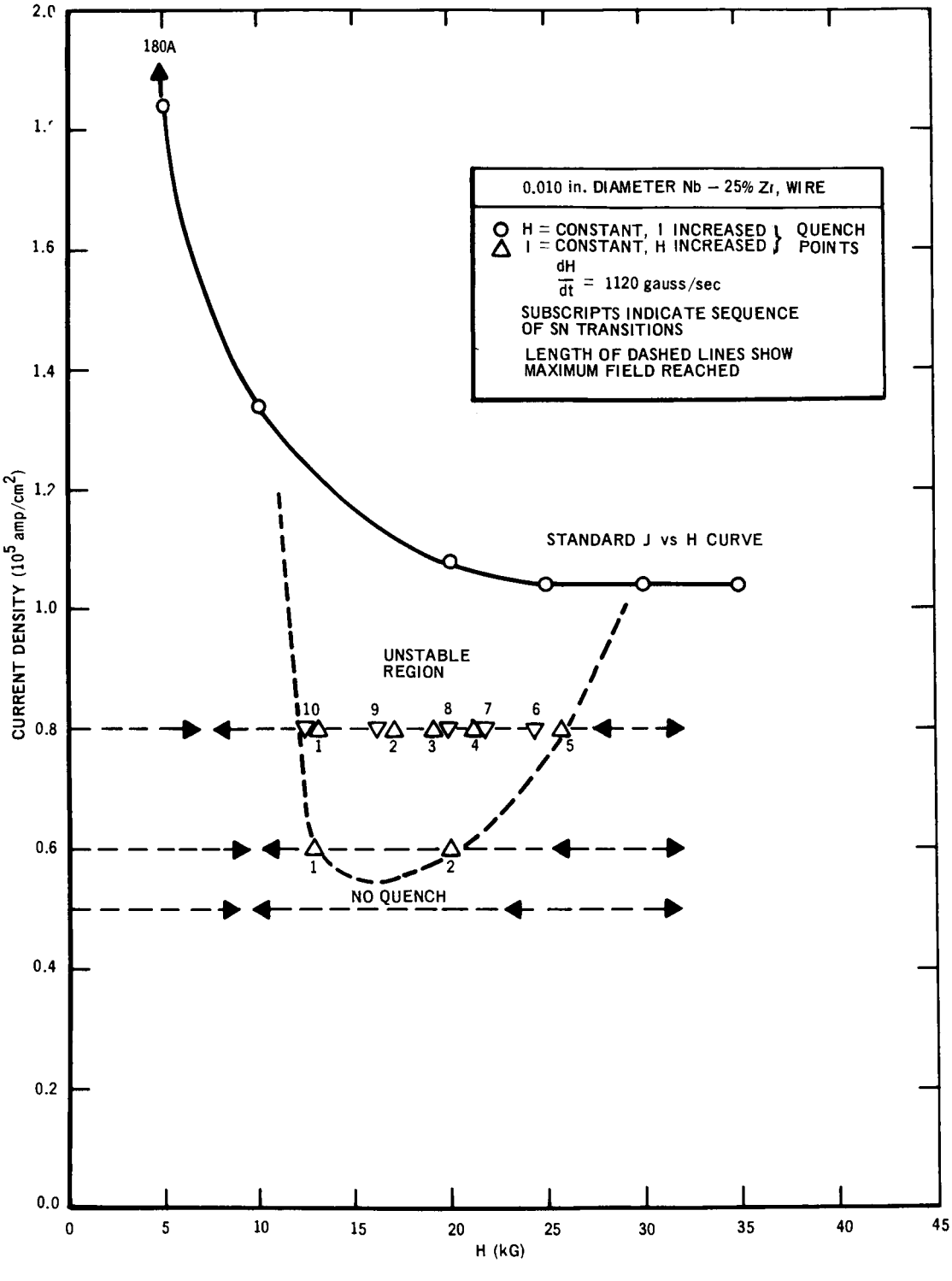

Figure 16. Example of Supercurrent Instability in Nb-Zr Wire, 0.010 in. Diameter, 4.2°K

The J_c versus H measurement for sample 9 (500°C - 300 min) was extended to 75 kG using facilities at ORNL.* This data is shown in Figure 12.

Sample 29 (400°C - 300 min) burned out upon testing, and only one data point (J_c = 1.3 x 10^5 amp/cm^2 at 30 kG) was obtained. This point agrees well with that of sample 26 (400°C - 45 min).

C. SUPERCURRENT STABILITY TESTS

1. Description

Supercurrent stability of the warm-aged Ti - 22 at. % Nb wire samples has been investigated. This measurement consists of testing a short wire sample carrying a dc current for super-to-normal (SN) transitions in a time-varying magnetic field. Unstable samples go normal at field-current values below the standard J versus H curve (defined in Section I. A.). For unstable superconductors, a region of instability can be found.[4, 5] For a typical Nb-Zr wire, this region is bounded in field between approximately 5 and 30 kG and in current density between a minimum of 5 x 10^4 amp/cm^2 and the standard J versus H curve, as illustrated in Figure 16.[4] Generally, for a particular material, the size of this region is dependent upon the rate of change of field, with the degree of instability increasing with increasing dH/dt. Also, and most important for our work, the size of the unstable region is material-dependent.[4]

The samples were the same as used in the J versus H tests discussed in the preceding section. The experimental circuitry is also the same as in the preceding tests except that the magnetic field current control was operated in the constant dH/dt mode instead of the constant current mode. The magnetic field could be increased or decreased at rates between 5 and 2000 gauss/sec.

The experimental sequence is as follows: After a sample current is established in zero field, the field ramp is initiated at the preset value of dH/dt. At some current-field value, the sample will become normal (resistive) and a voltage will appear across the sample. When this happens, the sample current

*See acknowledgments.

TABLE 2

SUPERCURRENT STABILITY OF HEAT-TREATED
0.010-in.-DIAMETER
Ti - 22 at. % Nb WIRE SAMPLES

Sample	Warm Aging Temperature (°C)	Warm Aging Time (min)	Stability: X Stable; Y Unstable to Field Reversal
2	200	10	Y
10		3000	X
25		36,000	nt*
18	250	10	nt
4		1000	X
3		3000	nt
24	300	300	nt
13		1035	X
15		3020	nt
17	350	103	X
22		300	X
14		980	X
26	400	45	X
19		100	X
29		300	nt
27	450	10	X
21		45	nt
28		100	X
30	500	30	nt
7		114	Y
9		300	X
20	550	34	X
16		3000	nt
8		2880	X
5	600	10	X
6		300	nt
12		1000	nt
23	650	3	nt †
11		34	nt
1		1560	nt

*No test

†J versus H curve too low to have instabilities, which occur for values of J and H above 5×10^4 amp/cm^2 and 5 kG respectively.

is turned off, and the field is held constant. If this SN transition occurs below the value expected from the standard J versus H curve, the sample current is again turned on, and the field sweep resumed, beginning at the field value of the preceding SN transition. This sequence is repeated until the standard J versus H curve is reached. The process is then reversed with dH/dt negative. This procedure is repeated with different combinations of J and dH/dt in order to define the unstable region.

2. Results

None of the Ti - 22 at. % Nb samples tested exhibited any supercurrent instabilities for values of dH/dt up to the maximum rate of 2000 Gauss/sec provided the field remained in the positive sense. Thus, the wires would not go normal until the standard J versus H curve was reached. However, SN transitions occurred in three samples, the 800°C starting material and samples 2 (200°C - 10 min) and 7 (500°C - 100 min) as the sense of the field became negative for values of dH/dt > 1000 Gauss/sec. If dH/dt was then made positive, a second transition was found to occur, not as H again became positive, but as H increased to ~+5 kG. There does not appear to be a correlation between the samples which showed the field reversal instability and the aging times and temperatures. Because of the seemingly random occurrence of these instabilities, we believe the cause is not basic to the superconductor but might be externally induced by movement of the samples as the field changes sense.

Test results are summarized in Table 2. Samples 6 and 12 (aged at 600°C) and samples 1, 11, and 23 (aged at 650°C) were not tested because their current densities were too low to have instabilities; i.e., $< 5 \times 10^4$ amp/cm^2 for H≤5 kG (see Figures 14 and 15). Since tested samples with similar heat treatments show absolutely no instabilities, it is unnecessary to test the samples marked "nt" (no test) in Table 2.

D. RESISTIVE UPPER CRITICAL FIELD MEASUREMENTS

1. Description

The resistive upper critical fields, H_r at 4.2°K, for the 30 ti-Nb wire samples were measured using pulsed-field techniques, as developed at Atomics International by Berlincourt and Hake.[1] In this method, a transverse sample is tested

in a pulsed-field solenoid. The experimental sequence is the following: a small sample current is established in zero field, then the solenoid field is pulsed with msec rise times. A voltage is observed across the sample due to the super-to-normal (SN) transition at the critical field of the test sample. As the pulsed-field decays, the sample undergoes a normal-to-super (NS) transition provided the transport current was not sufficient to propagate the normal region. The SN and NS transitions are not abrupt in Type II superconductors, but take place over several kilogauss, even for homogeneous samples.[1]

The experimental circuitry is illustrated in Figure 17.

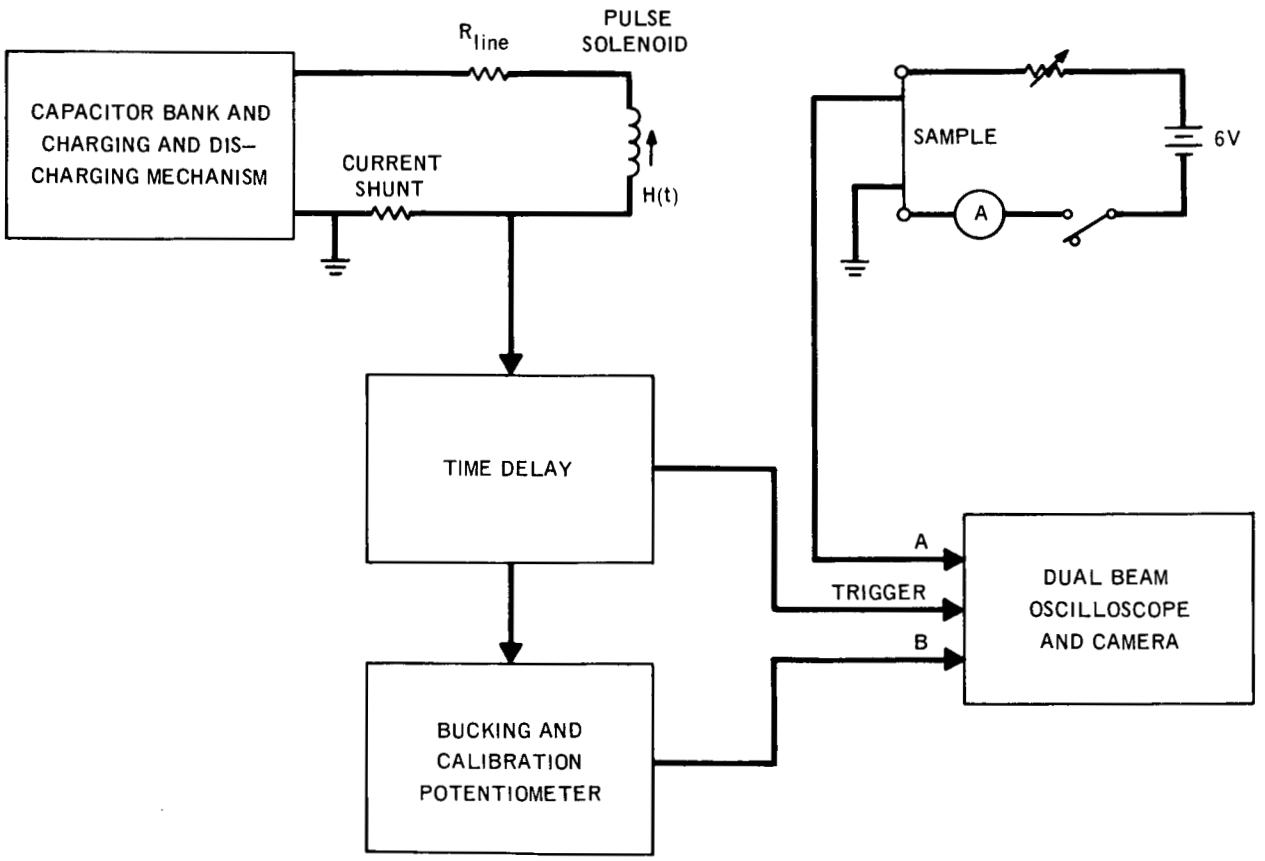

Figure 17. Experimental Circuitry for Resistive Upper Critical Field Tests

The pulsed magnet current (proportional to the field) and sample voltage are recorded with an oscilloscope. A time delay is used to trigger the sweep just prior to the SN transition, thereby permitting expanded sweeps of the transition voltage and field. The bucking potentiometer substracts a fixed voltage across the solenoid current shunt for higher field recording sensitivity.

Two pulses are recorded on each photograph: one with sample current flowing to record the SN transition, and the second with no sample current to measure the noise level due to dH/dt pickup. A typical pulse is shown in Figure 18a. The repeatability of the pulse is evident since the two solenoid field tracers are identical. Both the SN transition and the NS transition are well defined.

2. Results and Discussion

Data were taken at current levels of 0.005, 0.05, and 0.5 amp, corresponding to approximately 10, 100, and 1000 amp/cm^2, respectively. At each current level two pictures were taken: one showing both SN and NS transitions, and a second showing an exploded view of the SN transition.

The SN transition occurs at consistently higher fields than the NS transition. Evidently this discrepancy results from eddy currents and joule heating in the sample due to dH/dt,[1] thus the SN transition is taken as being more correct. From the above discussion, it follows that dH/dt must also cause H_r for the SN measurement to be less than H_{c2}, the upper critical field.

In analyzing the data, three fields are recorded. H_r is defined as the field at which half of the normal-state resistance is restored. The fields at which the onset and full restoration of resistance occur are labeled H_{ro} and H_{rf}, respectively. With the exception of sample 1 (650°C - 1560 min), the samples aged at 600 and 650°C exhibited double transition as typified in Figure 18b. Only a simple transition was observed in sample 1. These observations are discussed in Section I. F. in light of metallurgical examinations.

The data are plotted in Figures 5 through 15. Each graph shows the results for wires aged at the same temperature for different times. The data points represent H_r, while the bars indicate H_{ro} and H_{rf}. The results on 600 and 650°C samples are graphed separately in Figures 14a, b, and c and 15a, b, and c, to better illustrate the double transitions. The values of H_r are recorded in Table

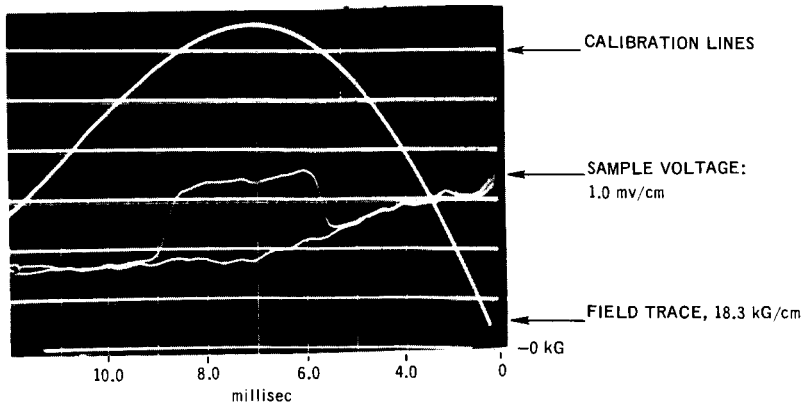

Figure 18. Typical SN Transition in Pulsed-Field, Sample 9, J = 109 amp/cm^2

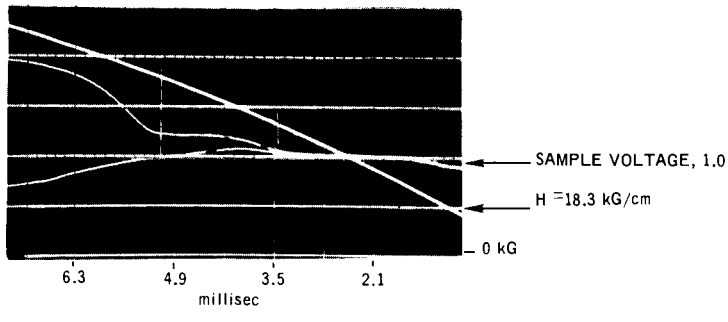

Figure 18b. Double Transition in Sample 5, J = 117 amp/cm^2

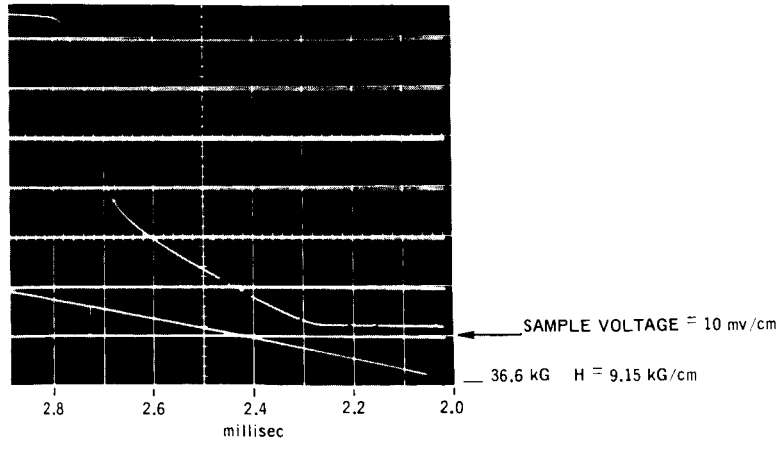

Figure 18c. Propagation of Normal Region Originating in Solder Joints

The values of H_r for the samples are plotted as a function of aging temperature in Figure 19 and as a function of aging time in Figure 20. The dashed portions in Figure 20 are extrapolations based on the solid line data.

Often, at current densities of $\sim 10^3$ amp/cm^2, normal regions propagate along the wire; a typical result is shown in Figure 18c. In this figure, the sample voltage (V_s) increases abruptly as the normal region propagates past one voltage probe. If H were constant, V_s should increase linearly.[6] However, since H is increasing, d^2V_s/dt^2 should be positive, which is the case. The average propagation velocity (ignoring the change in H) is reasonable, about 4 m/sec. The initial normal region evidently results from heating at the solder joints between the sample and the current leads and propagates if the current density is large enough.

From Figure 18c, the expected SN transition occurs at ~0.7 msec, a time too short to be due to a propagating normal front from the joints. Therefore, the magnetic SN transition is a measure of H_r.

E. CRITICAL TEMPERATURE MEASUREMENTS

1. Experiment

The critical temperatures (T_c) of the 30 Ti-Nb wire samples have been measured by observing the onset (and disappearance) of resistance as a function of temperature. The sample temperature probe is shown in Figure 21. Up to 8 wire samples are soldered to the relatively massive copper heat sink in which are embedded two carbon resistor thermometers. The large copper solder block is electrically common to all samples and is soldered to the heat sink to provide good thermal contact. The opposite end of each sample is soldered to a small copper block which is attached to the heat sink with an alumina filled epoxy (Stycast 2850 FT). The epoxy electrically insulates the floating ends of the samples while providing some thermal contact to the heat sink. A low temperature solder (158°F) is used to prevent annealing of the wire or overheating the carbon thermometers.

The heat sink is bolted to a copper can which is soldered to the stainless steel tube. The bottom 19.5 in. of the assembly is thermally insulated in the radial direction. All electrical leads pass down the tube and are thermally grounded to the copper can with the Stycast epoxy. The probe is connected

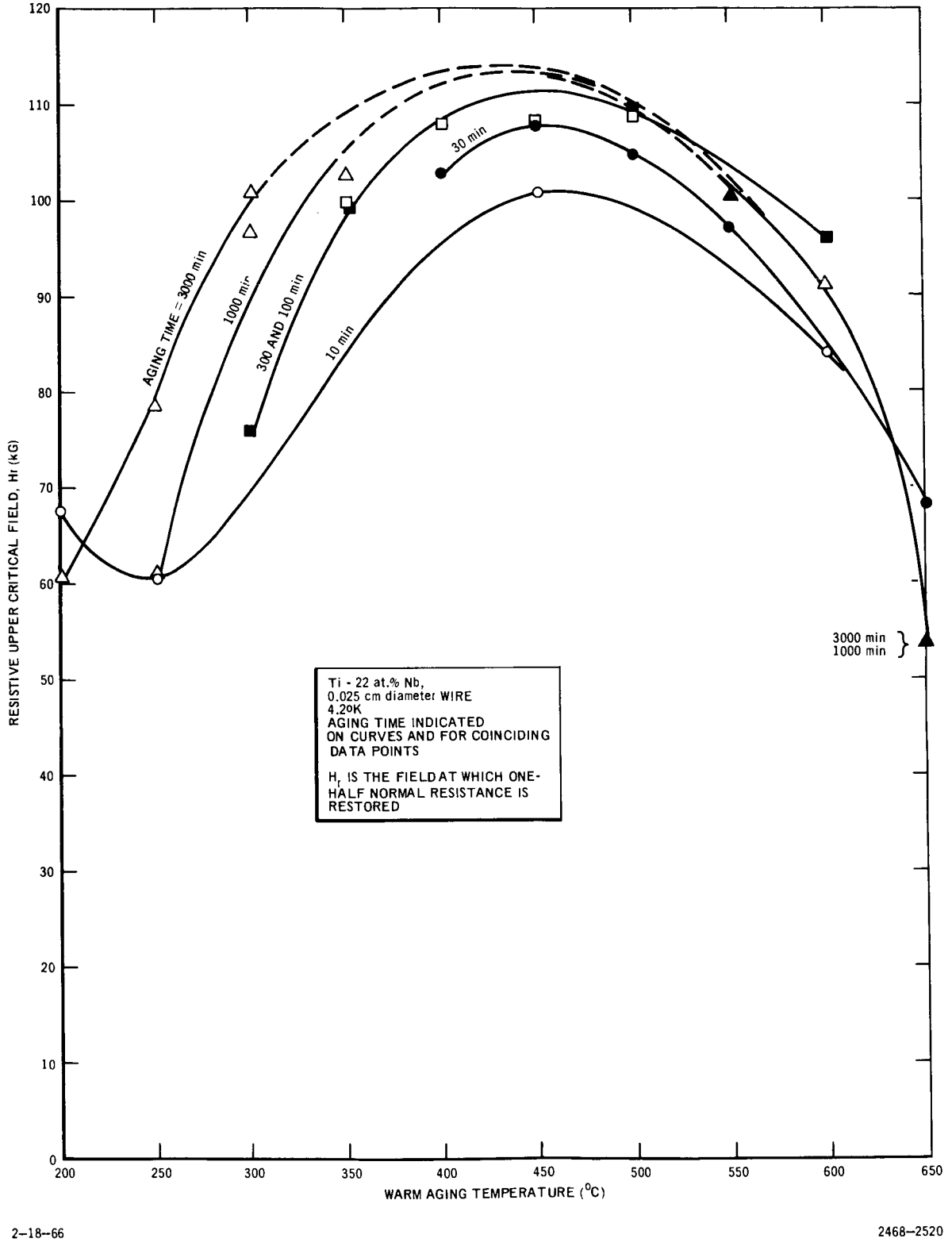

Figure 19. Resistive Upper Critical Field at 4.2°K of Ti - 22 at.% Nb as a Function of Warm Aging Temperature for Different Aging Times

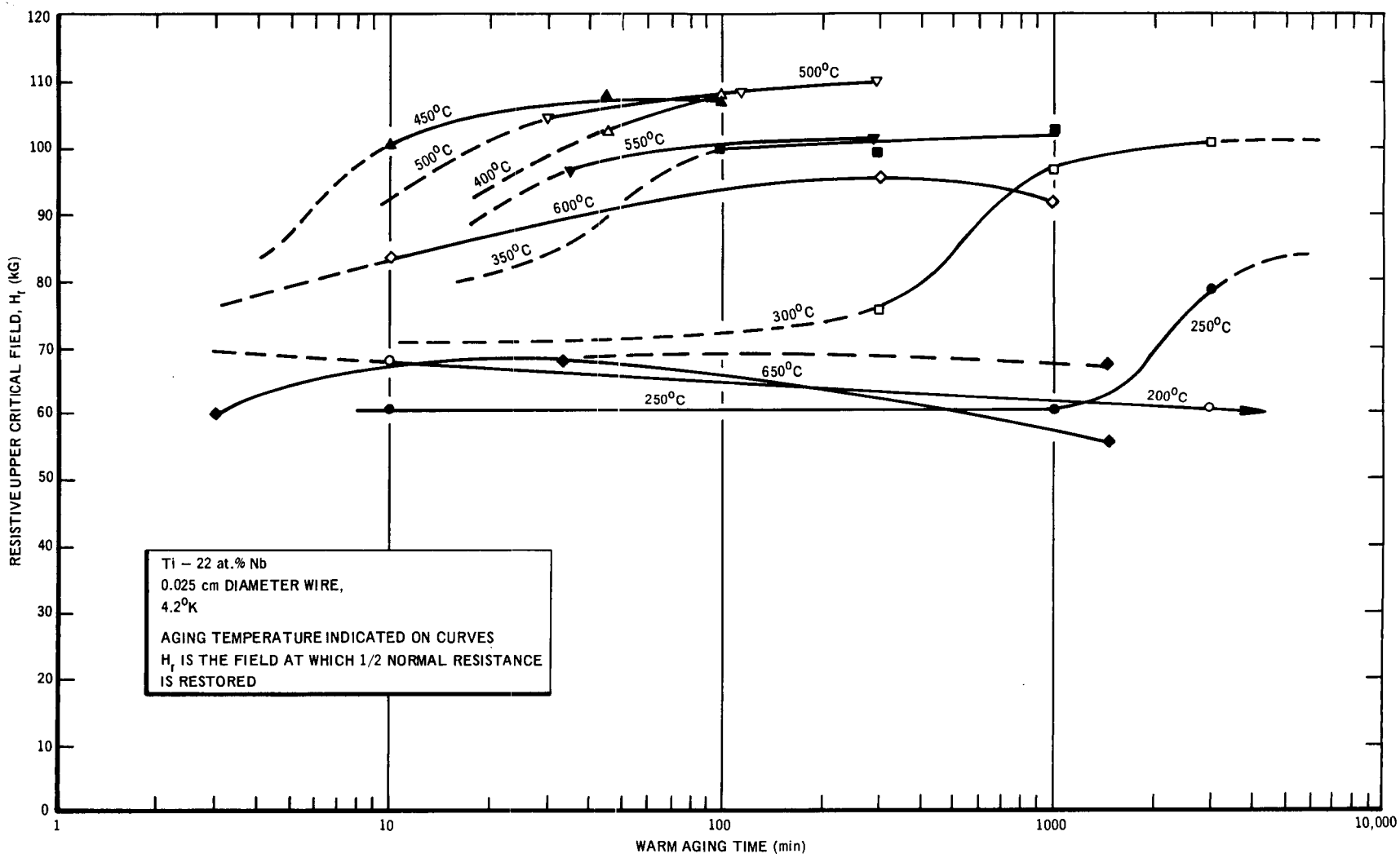

1–14–66

2468–2521

Figure 20. Resistive Upper Critical Field at 4.2°K of Ti - 22 at. % Nb as a Function of Warm Aging Temperature for Different Aging Times

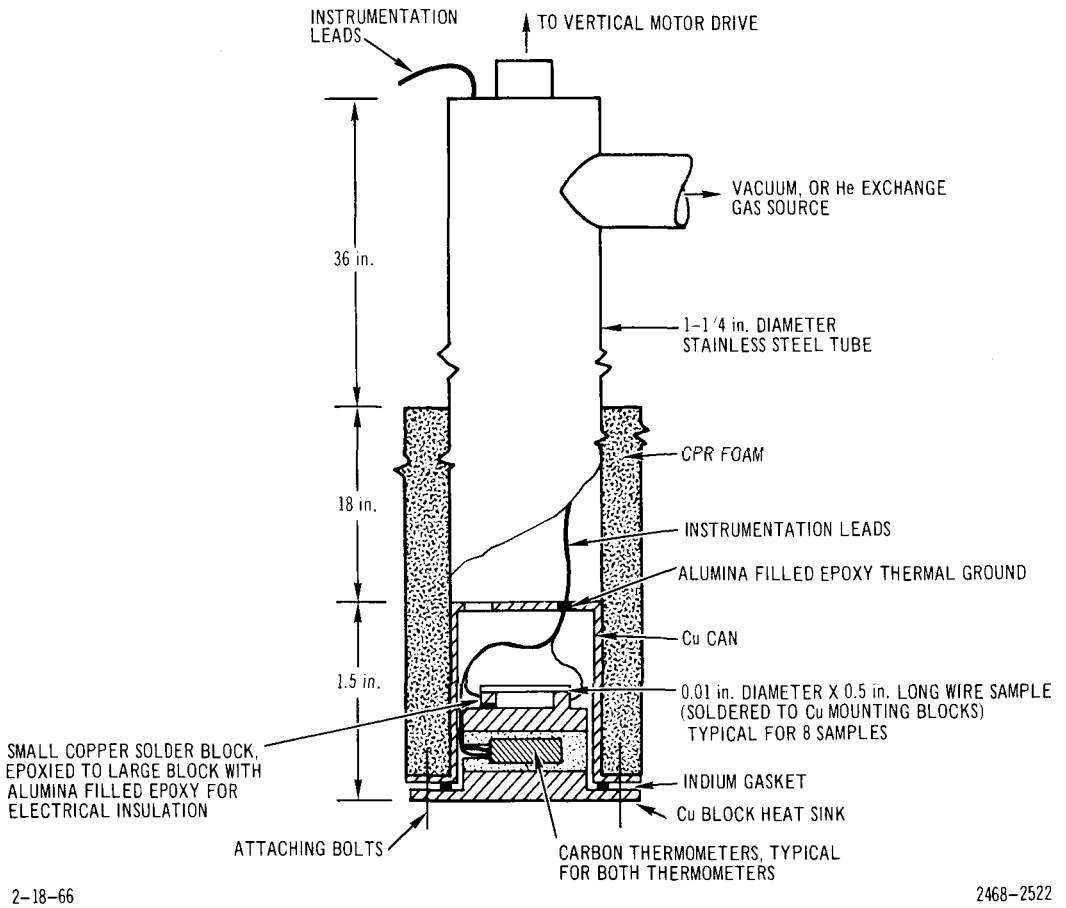

Figure 21. Sample Probe for T_c Measurements

through rack and pinion gearing to a reversible, variable speed, Bodine motor. Temperature is fixed by the height of the bottom surface of the heat sink above a liquid helium bath and is continuously varied by raising (or lowering) the probe with the Bodine motor. The rate of change of temperature can be varied from 0 to ±2°K/min.

In this apparatus, a sizable amount of heat can be conducted down the stainless tube and copper lead wires, and it is the role of the insulation and copper can to hold the temperature gradient across the sample to reasonable limits. In practice, it was found that the insulation must adhere well to the tube to prevent helium vapor from passing between the tube wall and the insulation,

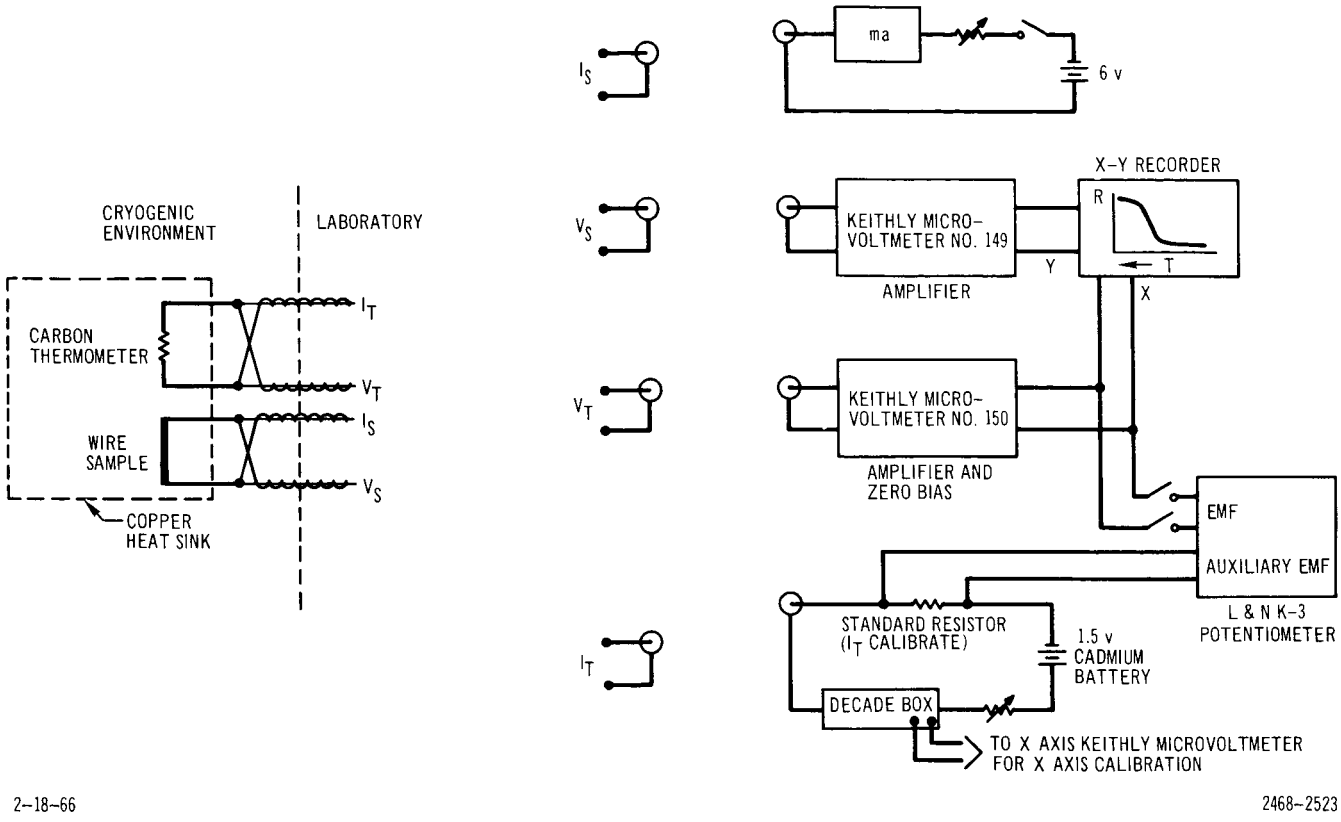

Figure 22. Block Diagram of T_c Experiments

thus creating a relatively large temperature gradient (~1°K/cm) along the copper can. A CPR Foam, which is poured around the tube using a mold to constrain the foam, worked well. A block diagram of the experiment is shown in Figure 22. Sample current is supplied by a 6-volt automobile battery. Voltage across the sample is amplified by a Keithly Model 149 microvoltmeter which drives the Y axis of a Mosley 2D X-Y recorder. A relatively large sample current of 300 μa is necessary to achieve sufficient sensitivity over the system noise of 1 μv peak-to-peak. Carbon resistor current of 10 μa is supplied by a 1.5-volt cadmium battery and accurately monitored with a Leeds and Northrop K-3 potentiometer. The voltage across the carbon resistor is amplified with a Keithley Model 150 microvoltmeter which drives the X axis of the X-Y recorder. A decade box in series with the thermometer current circuit is used to calibrate the X-Y recorder directly in ohms and to maintain constant resistance in the circuit during a run. With this apparatus, a direct plot of sample resistance versus carbon resistance (temperature) can be made.

TABLE 3

CRITICAL TEMPERATURES OF Ti-Nb SAMPLES AND 800°C STARTING MATERIAL

Temperature (°C)	Time	Sample	T_c (°K)	T_o (°K)	T_m (°K)	$\Delta T = T_m - T_o$
-	-	800°C	6.98	6.32	7.22	0.90
200	10	2	6.93	6.83	7.06	0.23
	3000	10	6.49	6.43	6.61	0.18
	36,000	25	6.47	6.40	6.59	0.19
250	10	18	6.78	6.64	6.96	0.32
	1000	4	6.51	6.45	6.66	0.21
	3000	3	7.55	7.43	7.72	0.19
300	300	24	7.20	6.90	7.37	0.47
	1035	13	8.50	8.44	8.61	0.17
	3020	15	8.70	8.66	8.83	0.17
350	103	17	8.38	8.32	8.53	0.21
	300	22	8.48	8.40	8.71	0.31
	980	14	8.89	8.83	9.07	0.24
400	45	26	8.26	7.67	8.50	0.83
	100	19	8.67	8.62	8.85	0.23
	3000	29	NA*	NA	NA	NA
450	10	27	8.18	8.09	8.40	0.31
	45	21	8.61	8.57	8.80	0.23
	100	28	9.75	8.69	8.94	0.25
500	30	30	8.51	8.36	8.62	0.26
	114	7	8.60	8.51	8.71	0.20
	300	9	8.81	8.74	8.92	0.18
550	34	20	8.16	7.93	8.44	0.51
	3000	16	8.32	8.14	8.54	0.40
	2880	8	8.51	8.38	8.66	0.28
600	10	5	7.53	7.45	7.77	0.32
			7.33	7.25	7.45	0.20
	300	6	8.19	8.00	8.38	0.38
			7.92	7.83	8.00	0.17
	1000	12	8.03	7.77	8.40	0.63
650	3	23	6.79	6.56	7.29	0.73
			6.38	6.15	6.56	0.41
	34	11	6.89	6.73	7.52	0.79
			6.66	6.60	6.73	0.13
	1560	1	6.70	6.60	6.86	0.25

*Not Applicable

The two carbon resistors were used to measure the temperature according to the relationship[6]

$$T = B(\log R + K \log^{-1} R + A)^{-1} \quad \ldots 1$$

where T is temperature, R is resistance, and A, B, and K are empherical constants.[7] A, B, and K were experimentally determined by measuring resistance at liquid hydrogen boiling point, hydrogen triple point, and liquid helium boiling point (HeBP). Due to the inherent lack of repeatability of carbon thermometers upon thermal cycling between 300°K and liquid helium temperatures, the resistors were calibrated at the HeBP at the beginning and end of each series of runs. Percent deviation between these HeBP calibrations and that given by the initial calibration were assumed to apply to all temperature measurements during a particular run and measured resistances were adjusted accordingly. The maximum deviation in the HeBP resistance was 2%. This adjustment assumes that the shape of the calibration curve does not change but should be a reasonable first order correction.

The following procedure was used to test each sample. Temperature sweeps were begun with the sample in the superconducting state, and the probe was raised, increasing T, until normal resistance was restored and then lowered until the sample became superconducting. First, a broad temperature range was scanned to locate T_c. Then, the Keithly microvoltmeter was used to suppress the unwanted portions of the signal from the carbon thermometers, and the gain of the Keithly was increased to record the SN and NS transition on an expanded scale.

Calibration marks (in ohms) using the decade box as a reference are placed on the recording paper at the beginning and end of each sample test. The above sequence was repeated for 7 samples mounted on the carbon block to complete a series of runs. Each sample was tested twice to eliminate errors due to mounting, poor contacts, calibration, etc.

2. Results

The critical temperatures of the 30 ti-Nb samples as well as the 800°C starting material are listed in Table 3. T_c is taken to be the temperature at

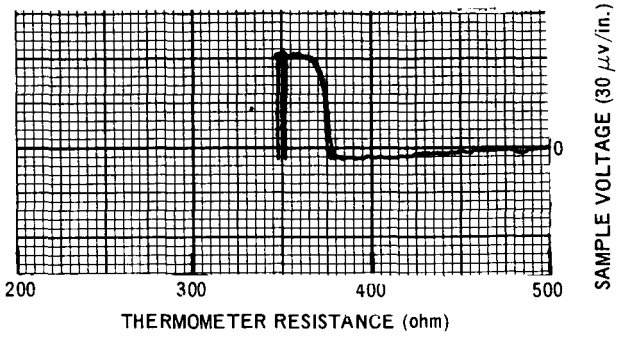

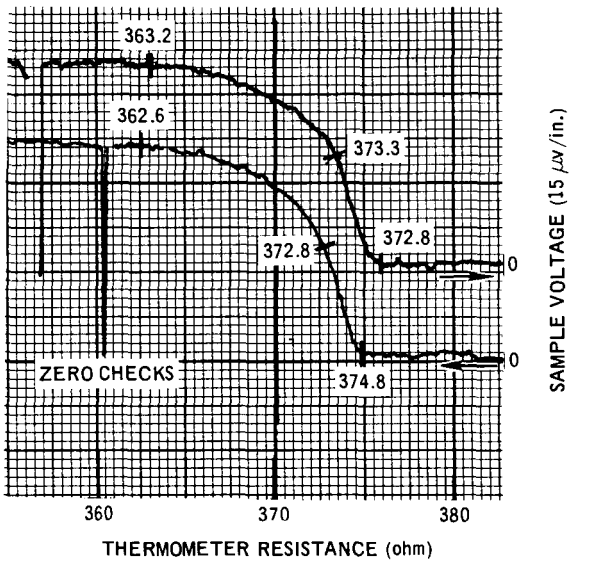

SAMPLE NO. 19
Ti-22 at.% Nb WIRE
0.010 in. diameter
AGED AT 400°C
FOR 100 min

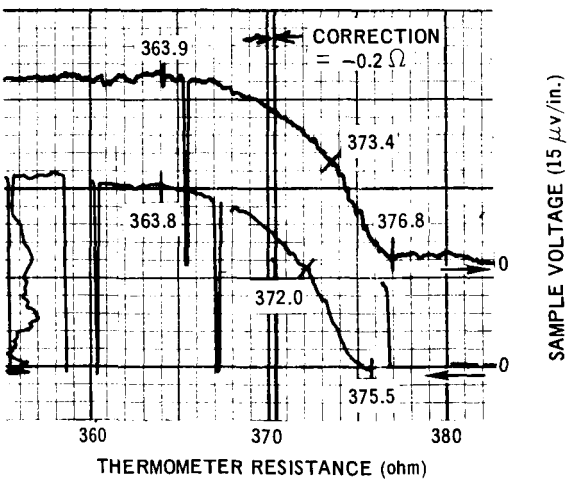

2–18–66

2468–2524

Figure 23. Recorder Trace of Thermal SN Transition in Ti-22 at. % Nb Heat Treated Wire

at which half of the normal resistance is restored; T_o is the temperature at which the onset of resistance is detected; T_m is the temperature at which resistance is fully restored; and $T_m - T_o$ is the transition width. These temperatures are the average of the 2 values found for each sample. A typical transition curve is shown in Figure 23. The upper curve is the first run to locate T_c. In the middle pair of curves, the Keithly microvoltmeter is used to suppress unnecessary temperature signal, and the X sensitivity is increased 10-fold to accurately determine the transition. The SN and NS transitions are indicated. Since the normal resistance versus temperature curve has a slight slope, the deviation from this curve at T_m is difficult to determine accurately. The before and after run calibration marks are also shown. The lower pair of curves shown in Figure 23 are the results of the second run on the sample.

The values of T_c for the samples are plotted as a function of heat treating temperature and time in Figures 24 and 25. These curves are of the same shape as Figures 19 and 20 of H_r versus the same parameters. As in the case of the H_r measurements, broad double transitions were observed in samples aged at 600 to 650°C, with the exception of sample 12 (600°C - 1000 min) and sample 1 (650°C - 1560 min).

3. Discussion

The two major sources of error are the absolute accuracy of the carbon resistance thermometers and the repeatibility of these thermometers upon thermal cycling between room temperature and liquid helium temperatures. The T_c of Pb, permanently mounted on the heat-sink, served to estimate these errors. T_c of Pb was checked at the beginning and end of each series of runs; the results are listed in Table 4. The average value of T_c is 7.172 ± 0.013°K as compared to the presently accepted value of 7.193 ± 0.005°K.[8] The assigned error of 0.013°K is the standard deviation of the data. The standard deviation of the differences of the two measurements on each sample from the mean value for each sample is also 0.013°K. Thus, the repeatibility of the results is estimated to be $\leq \pm$ 0.02°K. The difference of 0.02°K between the measured T_c for Pb (7.172°K) and the accepted value of T_c (7.193°K) indicates the absolute accuracy of the temperatures. However, it is felt that the 0.02°K agreement is somewhat fortuitous, and an assigned accuracy of ±0.1°K is more realistic for these readings.

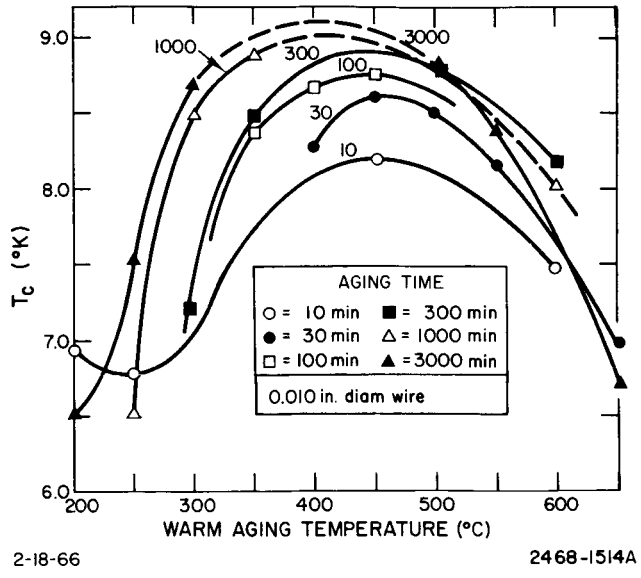

Figure 24. Critical Temperature of Ti - 22 at.% Nb as a Function of Warm Aging Temperature for Different Aging Times

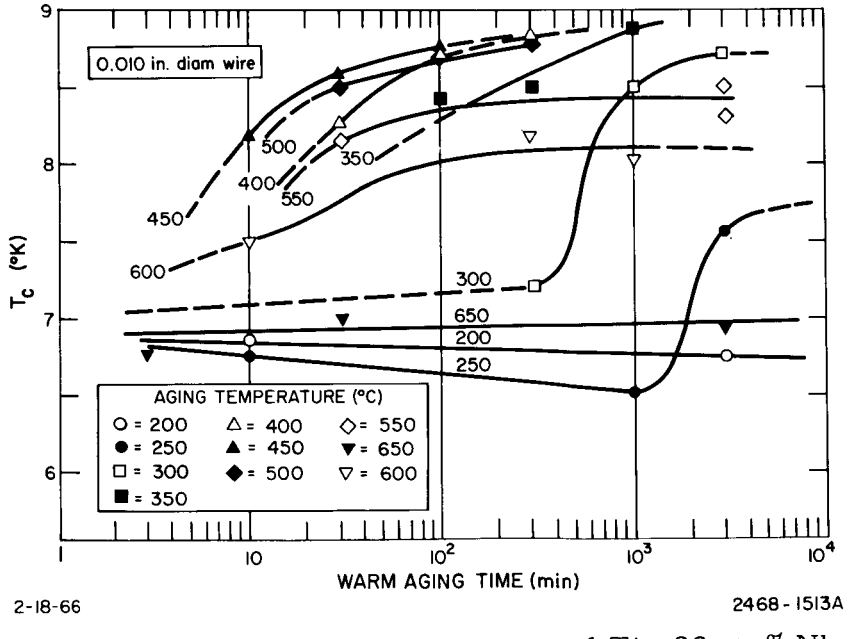

Figure 25. Critical Temperature of Ti - 22 at.% Nb as a Function of Warm Aging Time for Different Aging Temperatures

TABLE 4

TRANSITION TEMPERATURES OF LEAD STANDARD

T_c (°K)	T_c (°K)	T_m (°K)	ΔT (°K)
7.143	7.134	7.152	0.018
7.170	7.158	7.182	0.024
7.160	7.149	7.170	0.021
7.162	7.151	7.174	0.023
7.178	7.171	7.184	0.013
7.178	7.171	7.185	0.014
7.185	7.180	7.190	0.010
7.182	7.175	7.190	0.015
7.175	7.167	7.183	0.016
7.184	7.176	7.192	0.016

$\overline{T}_c = 7.172 \pm 0.013°K$

$\overline{T}_o = 7.163 \pm 0.014°K$

$\overline{T}_m = 7.180 \pm 0.013°K$

$\overline{\Delta T} = 0.017°K = \Delta\overline{T}$

T_c = temperature at which half of normal resistance is restored

T_o = temperature at which onset of resistance is detected

T_m = temperature at which resistance is fully restored

ΔT = temperature gradient

The maximum temperature drop across the sample can be estimated by assuming that the width of the SN transition is due entirely to a temperature gradient along the Pb sample. This ΔT is 7.180 - 7.163 = 0.017°K. Considering the thermal resistances of the sample and apparatus, the ΔT across the Ti-Nb samples is estimated to be ~0.05°K. It should be noted that a He exchange gas was required to achieve this small temperature gradient.

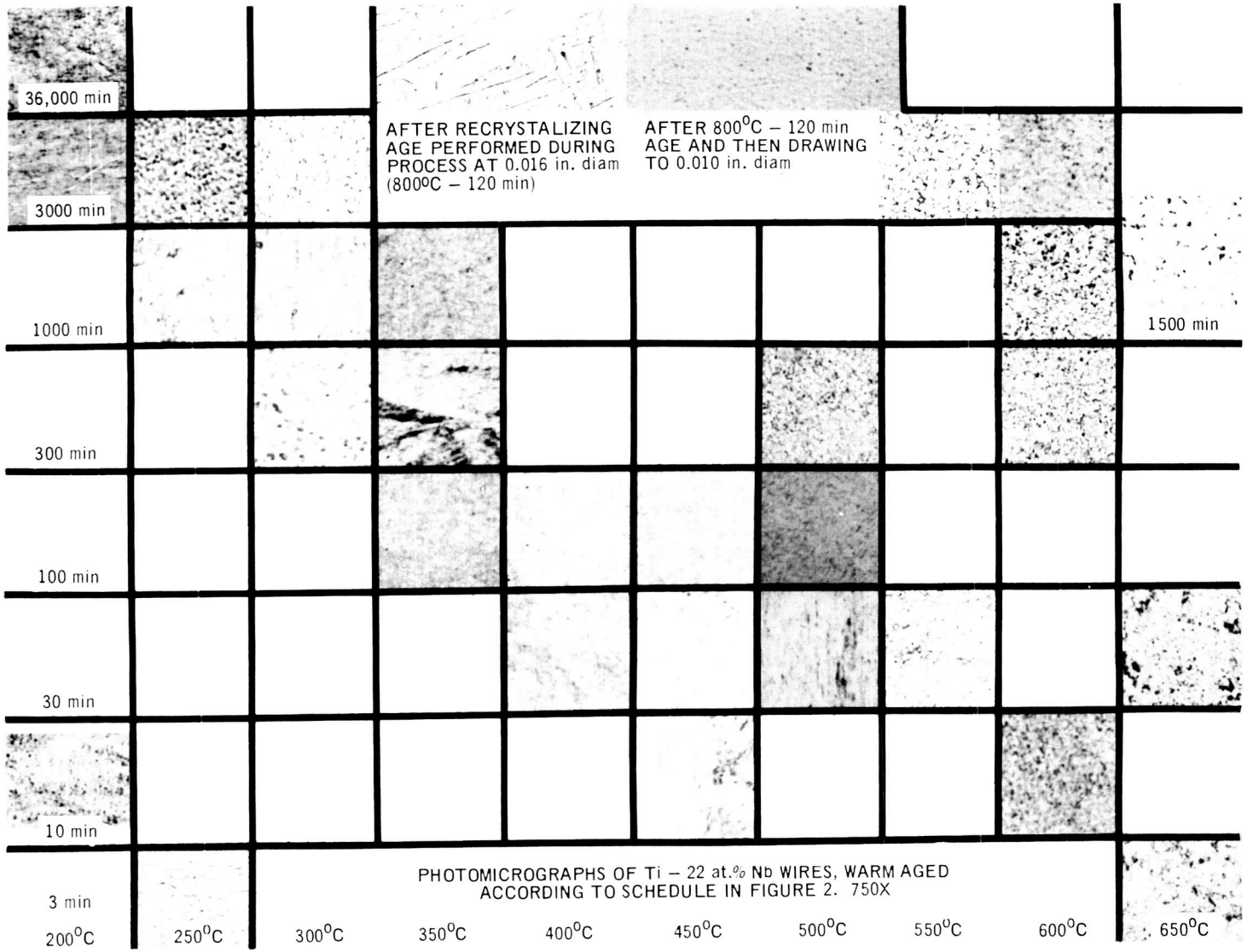

Figure 26. Photomicrographs of Warm Aged Ti - 22 at. % Nb Wire Samples Arranged According to Aging Temperature and Time.
(In process and 800°C aged wire photomicrographs also shown) (750X magnification)

The Pb used in the experiment exhibited a room temperature to liquid helium temperature resistance ratio of 500. Thus, the ΔT in the SN transition might be due partially to impurities and strain and not entirely to a temperature gradient along the sample. This fact would reduce the 0.05°K estimate of ΔT along the Ti-Nb wires. The Pb impurity should not affect the value of T_c within the accuracy of the carbon thermometers.

Maximum power generation levels in the carbon thermometers, Ti-Nb wires, and Pb strip are 5×10^{-8}, 10^{-8}, and 10^{-7} watts, respectively. The maximum temperature rise due to the above heat generation is < 0.001°K.

It is necessary that the sample be close to thermal equilibrium as the probe is raised and lowered. The hysteresis in the SN and NS curves indicates the degree of equilibrium, and the average hysteresis of all runs was 0.08°K. This equilibrium is achieved with a $dT/dt \leq \pm 0.2$°/min.

The suppression of T_c due to the sample current is negligible.

F. METALLURGICAL AND PHYSICAL PROPERTIES

The results and trends of microstructure, hardness, resistivity, and composition tests are presented below. Correlations between sets of results are postponed until the next section.

1. Microstructure

The microstructures of the 30 samples are shown in Figure 26. The photomicrograph of the wire after 800°C aging shows recrystallization and possibly some martensite. Martensite formation is borderline in the 22 at. % Nb alloy.[9] The photomicrograph of the 800°C starting material shows the structure after cold drawing the 800°C warm aged wire to 0.010 in. diameter.

The remainder of the photomicrographs show the various samples after low-temperature aging. These show only small changes due to the low-temperature short-time agings. Precipitation of a second phase becomes evident as either time of temperature is increased. This precipitate becomes larger as aging temperature exceeds 500°C, becoming quite large at the highest temperature of 650°C. Intermediate aging temperatures (350 to 500°C) for moderate times produces a finely dispersed precipitate in contrast to the coarser precipitate at higher aging temperatures.

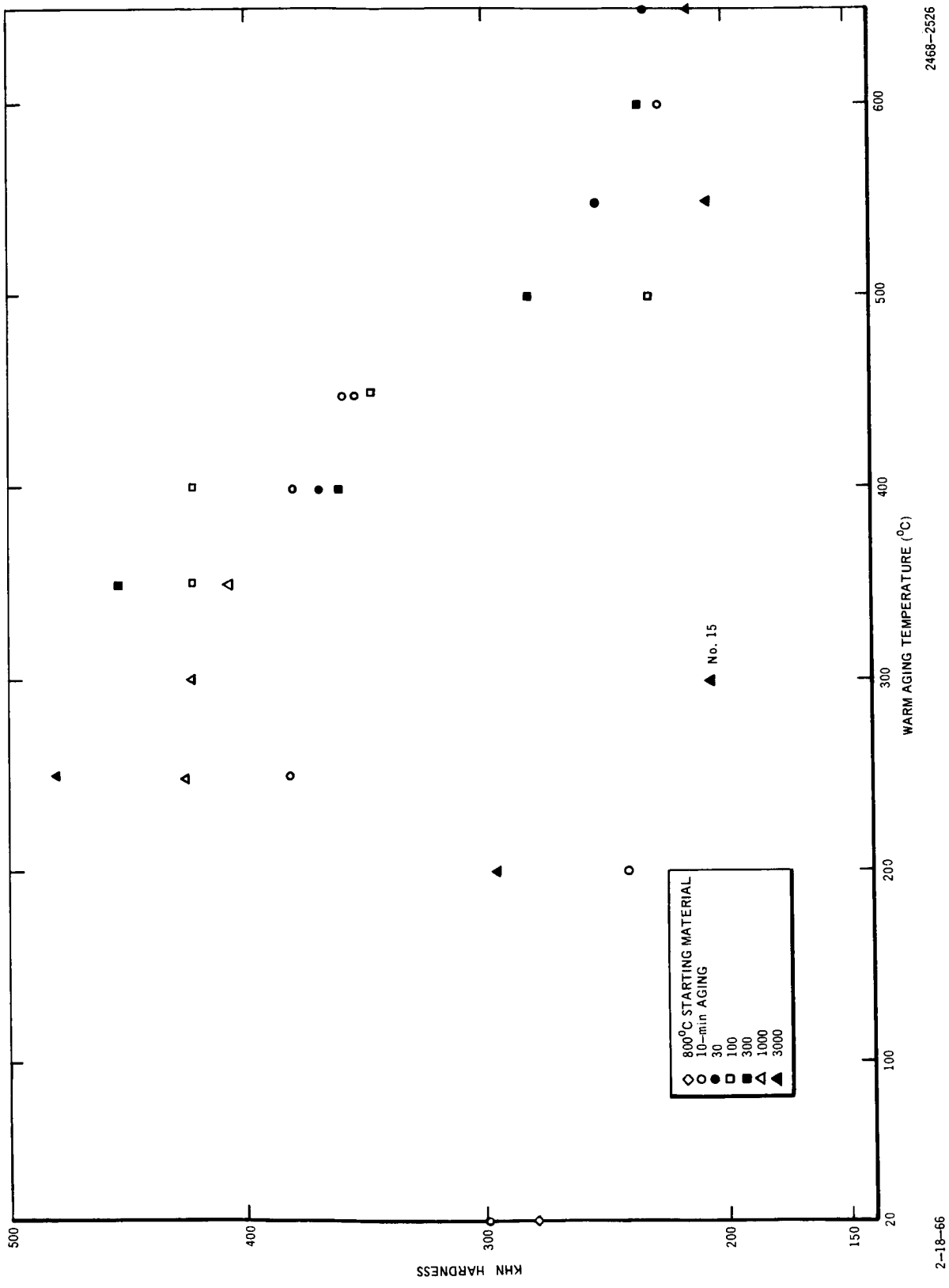

Figure 27. KHN Hardness of Ti - 22 at. % Nb Wires vs Aging Temperature

2. Hardness

KHN hardness measurements were performed on the 30 samples. The results are listed in Table 1 and graphed in Figure 27. These values are felt to be accurate to ±50 KHN points. The hardness values are not consistent, but do show a general trend: the values peak around 250 to 350°C and thereafter decrease with increasing temperature.

3. Normal-State Resistivity

Resistivity measurements were made at room temperature on the pre- and post-aged material (ρ_o and ρ_f, respectively). The normal-state resistivity at 4.2°K (ρ_n) was calculated from the voltage and current measurements in the pulsed-field tests at a current density of 10^3 amp/cm^2. The results are given in Table 1. Figures 28 and 29 illustrate qualitatively the variation of resistivity as a function of warm-aging temperature. Figure 28 shows the ratio of post-aging resistivity to pre-aging resistivity (ρ_f/ρ_o) as a function of aging temperature. The curves are drawn to indicate only general trends since the data is too sparse to be more exact. The results show a minimum in ρ_f/ρ_o around 450 to 500°C for short times. This minimum appears to occur at lower temperatures as aging time is increased. Figure 29 shows ρ_n/ρ_f versus aging temperature and has a minimum in the vicinity of 350 to 500°C. Values for samples 22 (350°C - 300 min.) and 6 (600°C - 300 min.) appear to be different from the general trend.

The largest source of error is in determining the area of the wires. Additional error is introduced in ρ_n because of error in accurately determining the distances between voltage probes. Errors are estimated to be 5% in ρ_o and ρ_f and 10% in ρ_n.

4. Composition of Phases

Results of Vetrano and Boom[2] and of x-ray diffraction analyses on the 30 samples show that the precipitated second phase was α-Ti and that continuous matrix was β - Nb. In addition to this information, it is useful to know the composition of the continuous (β - Nb) phase. This determination is not a straightforward process of finding the cell constant and looking up the concentration, because the cell constant of β-Ti-Nb only expands from 3.278 Å for 100% Ti to 3.294 Å for 100% Nb. The major portion of this change occurs between 60

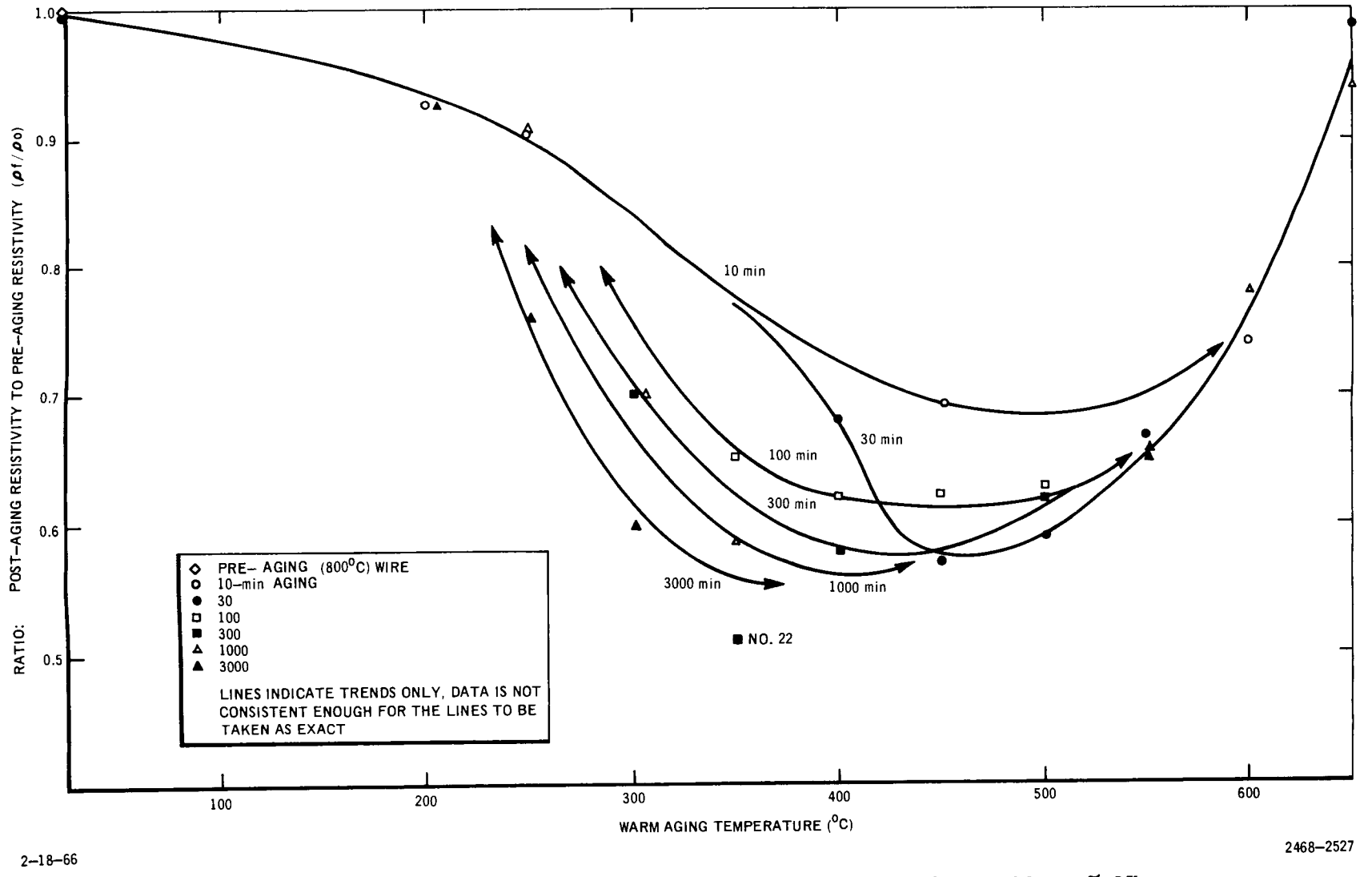

Figure 28. Ratio of Post- to-Pre-aged Resistivity of Ti - 22 at. % Nb Wires as a Function of Aging Temperature for Various Aging Times

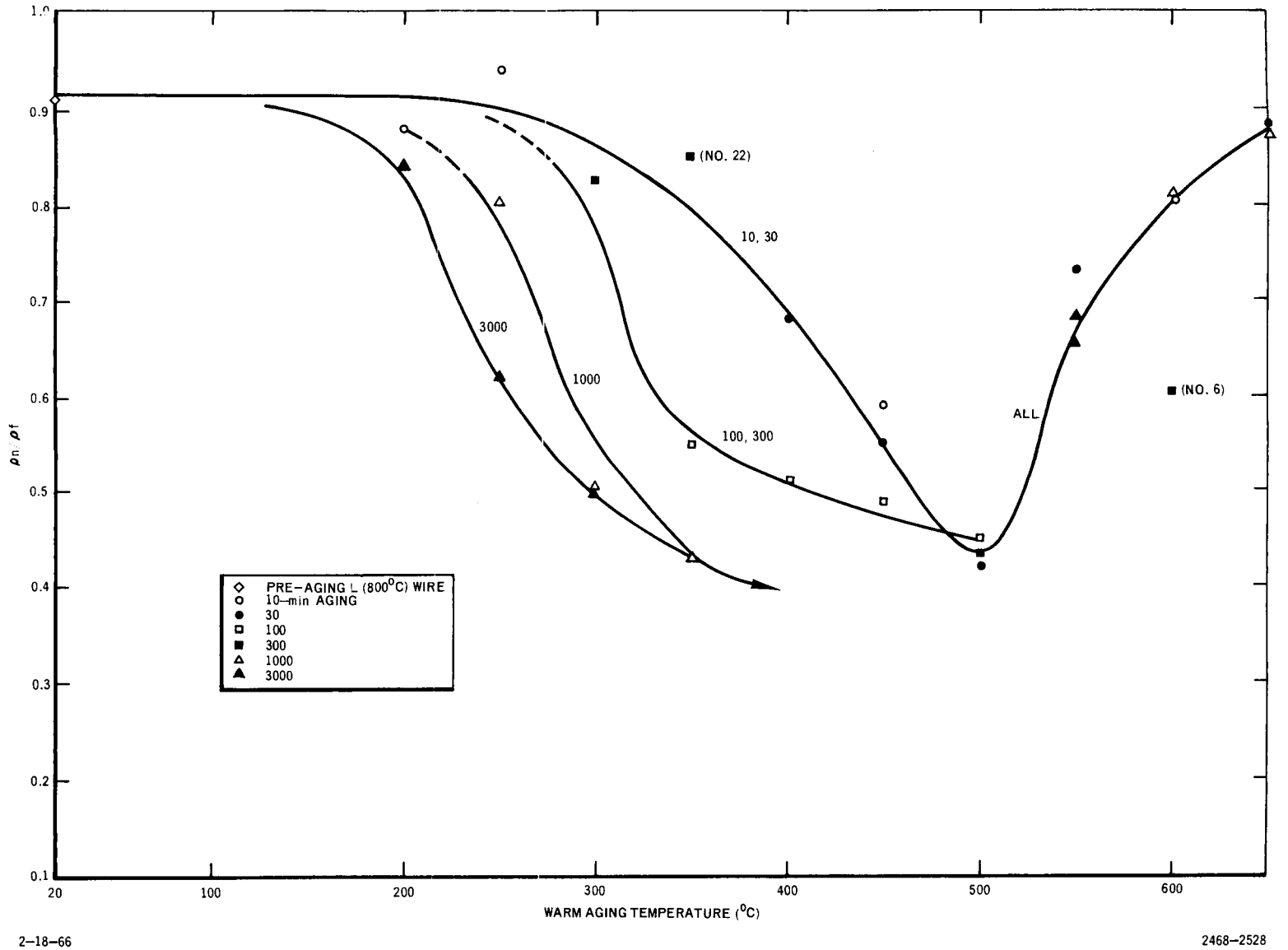

Figure 29. Ratio of Normal-State Resistivity (ρ_n) at 4.2°K to Room Temperature Post-Aging Resistivity (ρ_f) of Aged Ti - 22 at. % Nb Wires as a Function of Aging Temperature and Time

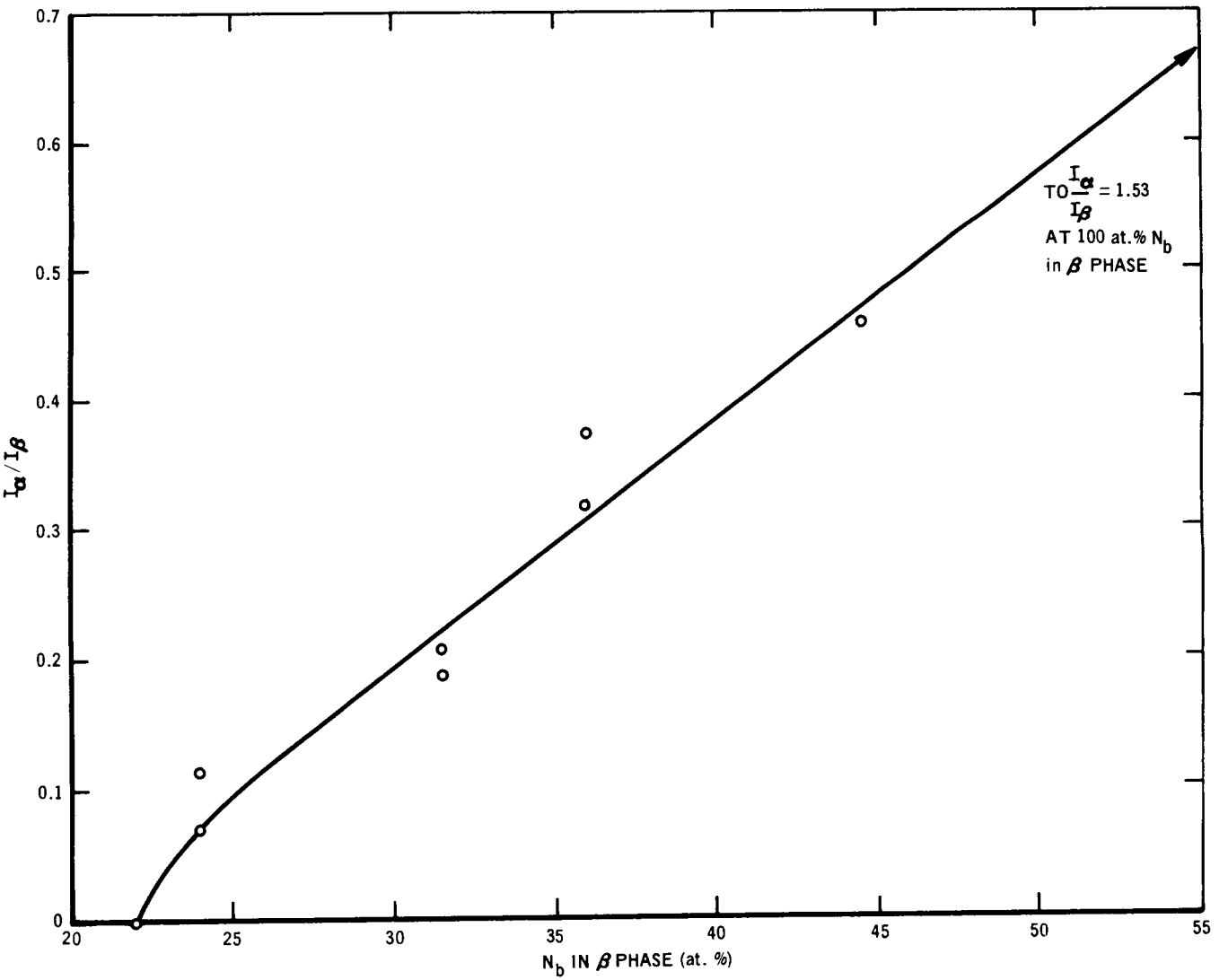

Figure 30. Calibration Curve: Ratio of Strongest Diffraction Peaks I_α for (011) α -Ti and I_β for (110) β -Nb versus at. % Nb in β -Phase of Two-Phase Ti - 22 at. % Nb

and 100 at. % Nb. The use of this technique is further handicapped by the fact that the diffraction lines from the samples are relatively broad. Therefore, another method had to be found. The best approach was to compare the relative intensities of the strongest diffraction peaks, (011) for α and (110) for β (hereafter called I_α and I_β), to a standard curve.

The samples for the standard curve were prepared using ingots of five different Nb concentrations. Filings were taken from each of these ingots, and the correct amount of α-Ti was added to produce an overall composition of Ti - 22 at. % Nb. The proper amount of Nb atoms were assumed to be in the α-Ti phase and were considered in calculating the material requirements to produce the correct overall 22 at. % Nb composition. These samples closely approximate the two-phase Ti-Nb alloy. The major error is that the 3 at. % Nb, which should be present in the α-Ti phase, is essentially replaced with Ti atoms. This substitution will reduce self-absorption of x-rays by ~1%, a negligible amount.

The standards were then analyzed with an x-ray diffractometer for I_α and I_β. The results are given in Table 5 along with the alloy concentrations. In three cases, samples were duplicated to estimate the precision, which turned out to be relatively poor. These differences in I_α / I_β could be due to stratification of the powders in the x-ray slide, resulting in different self-absorption between samples. In Figure 30 the results are plotted versus at. % Nb in the β-phase. The end point results from $I_\alpha = 0$ in the limit of all β-phase (at 22 at. % Nb). The error, as estimated from the scatter in the I_α / I_β points, is ±10% in Nb concentration.

X-ray diffraction patterns were run on each sample. The x-ray films were in turn analyzed with a recording densitometer to find the relative intensities of the (011) α-Ti and (110) β-Nb lines. The use of a densitometer was possible because the diffraction lines did not fully expose the x-ray film. The composition of the β-phase could then be found from Figure 31. These results are listed in Tables 1 and 4. If the α-Ti precipitate is assumed to be of equilibrium concentration, then, by knowing the overall composition and that of the α-phase, the atom and volume concentration of α-phase can be estimated. These results are also included in Table 6.

TABLE 5

RELATIVE INTENSITIES OF STRONGEST DIFFRACTION PEAKS OF α-Ti AND β-Nb FOR TWO-PHASE Ti - 22 at. % Nb STANDARDS

Sample	Nb in β Phase (at. %)	I_α / I_β
1A	24.0	0.069
1B	24.0	0.115
2A	31.4	0.209
2B	31.4	0.187
3A	36.0	0.318
3B	36.0	0.373
4	44.6	0.458
5	100.0	1.53

As stated above, these values of Nb concentration in the β-phase are accurate to ±10%.

The Nb concentrations of the β-phase are plotted on the equilibrium Ti-Nb phase diagram which is reproduced in Figure 31. The arrows between data points indicate increasing aging time. Several points show the Nb concentration decreasing as aging time increases. In all cases the decrease is well within the error limits, so it is impossible to attach significance to these reversals. At the higher aging temperatures, the Nb concentration agrees well with the equilibrium phase diagram. At the lower temperatures, the phase diagram is not known. The value of the Nb concentration in β-phase represents an average value.

G. CORRELATIONS OF EXPERIMENTS

1. H_r, T_c, Nb Concentrations and Microstructure

The resistive technique used measures H_r or T_c of the continuous phase in which superconductivity persists to the highest value of H_r or T_c. Any other phase, precipitated or continuous, will be normal and shunted by the

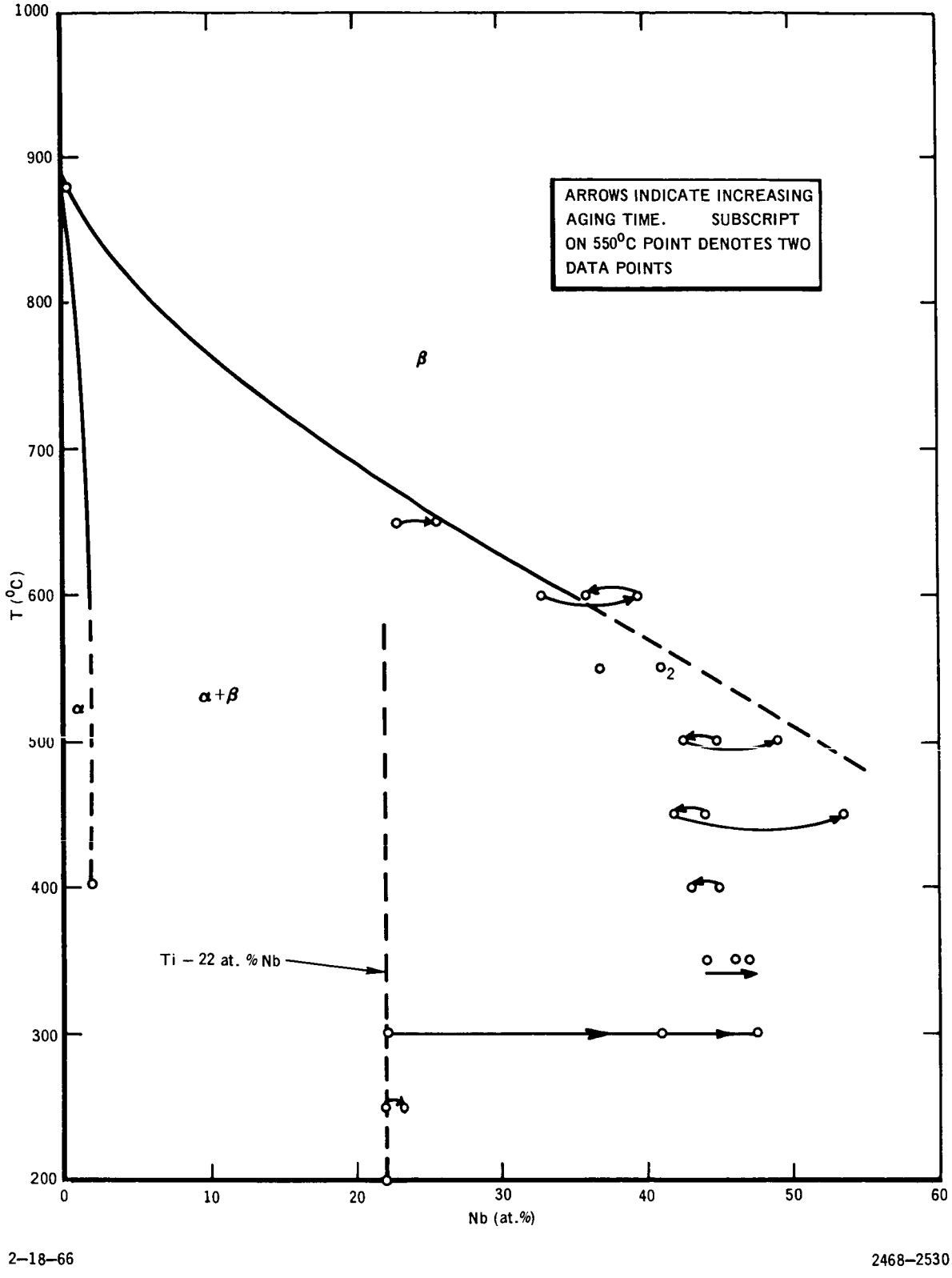

Figure 31. Equilibrium Ti-Nb Phase Diagram With Concentration of Nb in β-Phase of Warm Aged Wire Samples Included

TABLE 6

COMPOSITION AND CONCENTRATIONS OF α - AND β -PHASES OF WARM AGED Ti - 22 at. % Nb WIRES

Aging Parameters		Sample	Nb in β -Phase (at. %)	α -Phase (at. %)	α -Phase (vol. %)
Temperature (°C)	Time (Min)				
		800°C	22.0	0	0
200	10	2	22.0	0	0
	3000	10	22.0	0	0
	36,000	25	22.0	0	0
250	10	8	22.0	0	0
	1000	4	22.0	0	0
	3000	3	23.4	6	6
300	300	24	~23	5	5
	1035	13	40.8	48	50
	3020	15	47.5	56	58
350	103	17	44.2	53	55
	300	22	46.0	54	56
	980	14	46.7	55	57
400	45	26	44.9	53	55
	100	19	43.1	51	53
	300	29	NA	NA	NA
450	10	27	44.2	53	55
	45	21	41.7	50	52
	100	28	53.6	61	63
500	30	30	44.9	51	53
	114	7	42.6	51	53
	300	9	48.9	57	59
550	34	20	40.8	48	50
	3000	16	41.2	49	51
	2880	8	37.3	43	44
600	10	5	32.9	35	36
	300	6	39.6	47	48
	1000	12	35.7	41	42
650	3	23	~23	5	5
	34	11	23.4	5	5
	1560	1	25.7	16	16

superconducting phase. Since, in the foregoing section, it was shown that the β-phase was the continuous phase, the measured values of T_c or H_r correspond to this phase.

In view of this discussion, there appear to be two possible metallurgical configurations which would permit a double transition to be observed. If there were two phases, of which one must be continuous, and the phase with lower T_c or H_r goes normal, then the transport current could drive the other phase partially resistive. Since the current values used are too low to propagate a resistive region, the continuous phase with higher H_r or T_c remains partially resistive until H_r or T_c is reached; then the second transition is seen. The second possibility is that both phases are not continuous. Since the phases would then be essentially in series, a resistive region due to one phase becoming normal must produce a voltage.

The micrographs (Figure 26) of the 600 and 650°C samples show a precipitated, discontinuous phase in a continuous matrix: a result that tends to discount the probability of two noncontinuous phases. However, the fact that the 650°C materials only have a small amount of precipitate (5 to 16 at. % α-Ti from Table 6) casts doubt on the possibility that the continuous phase becomes partially resistive. An alternate explanation, and a variation on the second possibility, is that the continuous phase is formed of two concentrations of β-Nb structure. In any case, it is strongly felt that the highest T_c and H_r values are for the same composition; therefore, these values are paired.

It is interesting to compare H_r and T_c for Ti-Nb samples, which are generally heterogeneous, with published results on homogeneous Ti-Nb alloys. Figure 32 shows T_c versus Nb concentration. The curve is due to Hulm and Blaugher[10] for homogeneous, β-phase, Ti-Nb alloys. T_c values for the Ti-Nb samples are also plotted. Agreement with the data of Hulm and Blaugher is fair; our data is consistently higher at low values of T_c and consistently lower at high T_c. These differences do not appear to be due to errors in determining T_c since the combined error estimates for the two experiments are ~0.2°K. Also, differences in experimental methods would not be expected to lead to significantly different values of T_c. Hulm and Blaugher determined T_c from permability measurements, which is a bulk phenomena. Their transition widths were

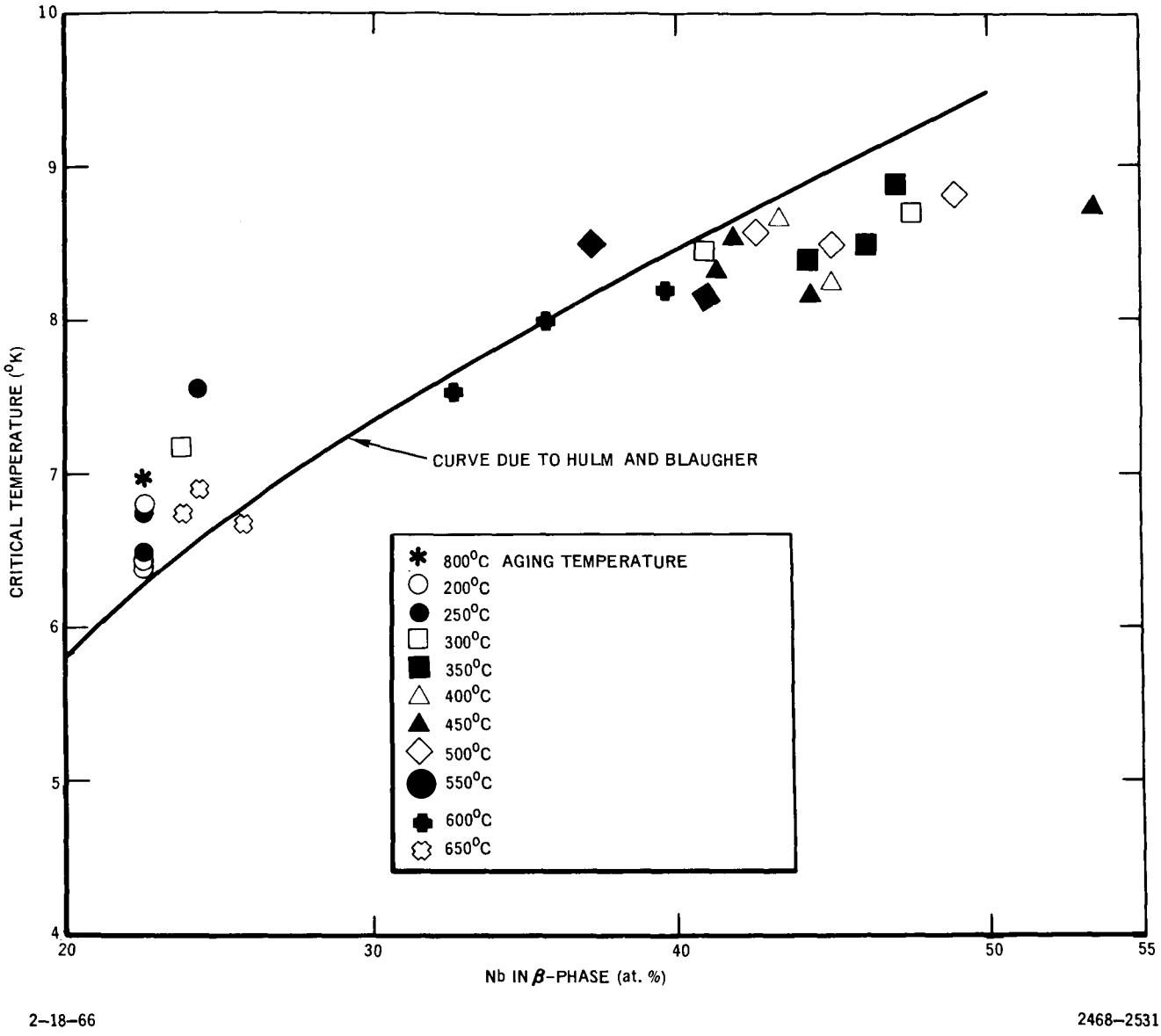

Figure 32. Critical Temperature of Warm Aged Ti - 22 at. % Nb Wires vs at. % Nb in β-Phase

≈0.1°K. The resistive techniques used in the work reported here selectively measure T_c for the highest continuous phase as discussed earlier. The differences between our T_c data and that of Hulm and Blaugher is felt to represent a true effect.

Figure 33 shows H_r for the Ti-Nb samples versus Nb concentration. The curve of H_r at 4.2°K is calculated from the critical field results of Berlincourt and Hake,[1] giving H_r at 1.2°K; and from the T_c data of Hulm and Blaugher,

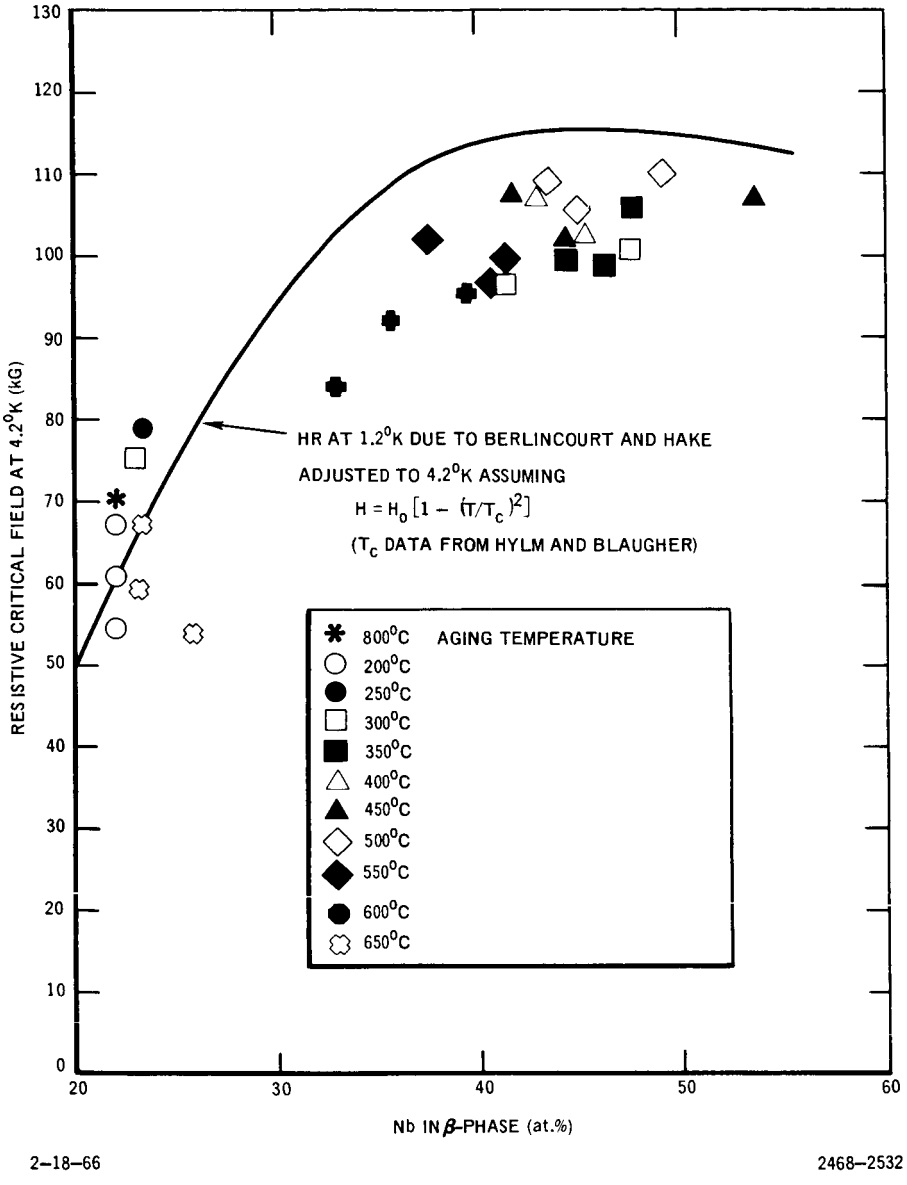

Figure 33. Resistive Upper Critical Field at 4.2°K of Warm Aged Ti - 22 at. % Nb Wires vs at. % Nb in β -Phase

using the parabolic approximation

$$H_r = H_o \left[1 - \left(\frac{T}{T_c} \right)^2 \right] , \qquad \ldots 2$$

where H_o is the upper critical field at 0°K, and H_r is measured at temperature T. This equation is a good approximation for the composition range of the aged samples since this is the range of validity[1] of Clogston's[11] paramagnetic spin-pairing consideration.

The H_r values for the aged samples agree, within experimental accuracy, with the homogeneous curve for samples with 22 to 24% Nb concentration. However, the data points lie below the homogeneous H_r curve at the higher Nb concentrations by 5 to 20%. As in the T_c measurements, these differences are felt to be not due to experimental errors or technique, but indicate true differences.

This reduction in T_c and H_r is felt to be due to the proximity of the α-phase precipitate. Such a result might be expected from theoretical considerations. If the distance between precipitate particles, i.e., the dimension of β-phase between inhomogeneities, is on the order of the coherence length, then the second phase might affect the superconducting properties of the β-phase. The coherence length is of the order of 10^{-4} cm, for homogeneous Type II superconductors and 10 to 100 times smaller for highly inhomogeneous alloys. Since the interference with inhomogeneity of the β-phase is under consideration, it appears correct to use the 10^{-4} cm value. The spacing between precipitate particles is estimated from the photomicrographs to be 10^{-4} cm for the course precipitate (550, 600, and 650°C samples and sample 9 at 500°C - 300 min). This spacing for the samples in the intermediate temperature range (350 to 500°C) is difficult to estimate because of the smallness and high density of the particle but is at least an order of magnitude less than for the coarser precipitate. Thus, these dimensions are the order of the coherence length, and the reduction of T_c and H_r could reasonably be due to the presence of the second phase.

2. Critical Current Density and Microstructure

A homogeneous Type II superconductor is unstable in the presence of a transport current. The unstable behavior results because the flux vortices, which permeate a Type II structure, are unstable under the pressure of J/B forces. To stabilize or "pin" the vortices it is necessary to introduce inhomogeneities in the material. These inhomogeneities are either normal or poorer superconductors than the matrix material. The Gibbs free energy ($\propto H_c^2$) of the

inhomogeneities is different than the matrix, and thus the inhomogeneities act as potential barriers opposing the Lorentz forces. In the aged Ti-Nb samples, the precipitation mechanism performs the flux pinning function.

Because of the dependence of current density on metallurgical structure, it is instructive to compare the resulting current densities for different samples with micrographs. The following qualitative correlations are apparent. Comparing J_c at 20 kG from Table 1 to the micrographs shown in Figure 26, current densities are highest (1 to 3 x 10^5 amp/cm^2) for the samples annealed at 30 to 500°C. These samples exhibit a small, dense precipitate. The T_c of wires aged at 550, 600, and 650°C have current densities $\leq 4 \times 10^4$ amp/cm^2, with $J_c \approx 2 \times 10^3$ amp/cm^2 for the 650°C wires. Micrographs of these wires show a coarser, less dense precipitate than the 350 to 500°C wires. The current densities ($\approx 5 \times 10^4$ amp/cm^2) and precipitate size and density of the 800°C starting material and the 200°C, 250°C, and 300°C wires are intermediate to the two cases discussed above. Sample 9 (500°C - 300 min) does not conform to these generalizations since $J_c \approx 10^5$ amp/cm^2, but the microstructure is quite similar to the 550 to 600°C samples which have low J_c. J_c seems to be highest for the most densely spaced inhomogeneities ($\approx 10^{-5}$ cm) and decreases as this spacing increases. Perhaps of significance is the fact that spacing of Abrikosov flux vortices at 20 kG is $\approx 0.3 \times 10^{-5}$ cm.[12]

J_c does not necessarily depend on the amount of precipitate. In the 200 and 250°C samples, J_c was $\approx 5 \times 10^4$ amp/cm^2, yet the amount of α-phase was < 5 at. % (see Table 6), the sensitivity of the x-ray determinations. In contrast, J_c for the 600 and 650°C wires was considerably lower (2 x 10^3 to 9 x 10^3) but had > 40 and > 4 at. % α-phase for the 600 and 650°C wires, respectively. Thus, the spacing of α-phase appears more important than the amount.

A more specific correlation between J_c and microstructure is unrewarding. For example, the 550 and 600°C micrographs are essentially the same, but the 550°C current densities are significantly higher. This result serves to illustrate that it is presumptuous to expect quantitative correlations between J_c and micrographs because other factors, unrevealed by the micrograph, could affect J_c. In conclusion, a quantitative correlation between current density and metallurgical structure requires a better understanding of the flux pinning and transport current mechanisms.

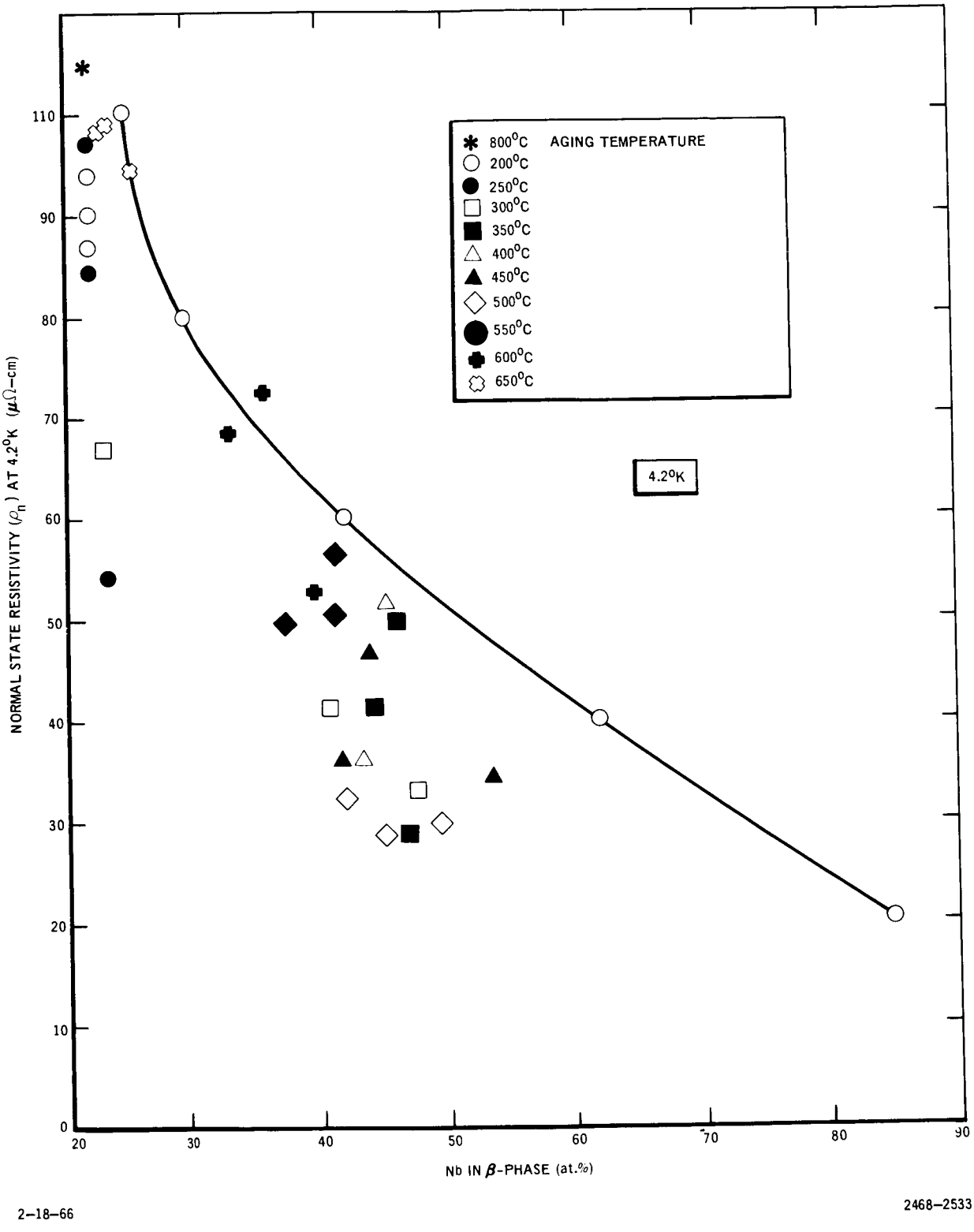

Figure 34. Normal State Resistivity at 4.2°K of Warm Aged Ti - 22 at. % Nb Wires vs at. % Nb in β -Phase

3. Resistivity and Nb Concentration

For homogeneous Ti-Nb alloys, normal-state resistivity is a single valued function of Nb concentration, as shown in Figure 34. The ρ_n values are plotted in this figure and, except for two points, are lower than the homogeneous values. This result simply means that the resistivity of the α-Ti phase is less than that of the β-phase.

H. CONCLUSIONS

Vetrano and Boom[2] showed that critical current density (J_c) and resistive upper critical field (H_r) can be improved in Ti - 22 at. % Nb by warm aging in the two-phase region. Their studies have been substantially expanded in the work presented in this report, and the results demonstrate that H_r and T_c (critical temperature) of warm aged Ti - 22 at. % Nb are functions of the composition of the continuous phase of the alloy. In addition, the flux pinning effect of the α-Ti precipitate (observed by Vetrano and Boom[2]) has been qualitatively correlated with precipitate spacing.

Thus, the superconducting properties of Ti - 22 at. % Nb pertinent to superconducting magnet design (J_c, H_r, and T_c) can be varied in a predictable manner which is summarized below. The Ti - 22 at. % alloy is heat treated in the two-phase region to precipitate flux pinning inhomogeneities (increasing J_c) and change the composition of the continuous matrix. The final alloy composition is chosen to give the desired value of H_r according to the homogeneous H_r versus composition curve. (The results of this work show that only ~90% of the maximum H_r will be attained, presumably because the precipitated phase suppresses H_r.) Since a range of times and temperatures will produce the desired composition (see Figure 33), the required heat treatment must then be based on T_c and J_c requirements.

Although this work is restricted to the Ti-Nb system, the method of optimizing the high field superconducting properties should be applicable to most of the binary transition metal alloy systems, and in particular to systems such as the Ti - V system, which have similar phase diagrams to Ti-Nb.

II. SUPERCONDUCTING WIRE LOOP

A. DESCRIPTION

The object of this experiment was to search for rapid or catastrophic flux penetration into a one-turn loop of Nb - 25% Zr wire. The loop and search coils were orientated perpendicular to a time-varying magnetic field and secured with a Teflon holder as shown in Figure 35.

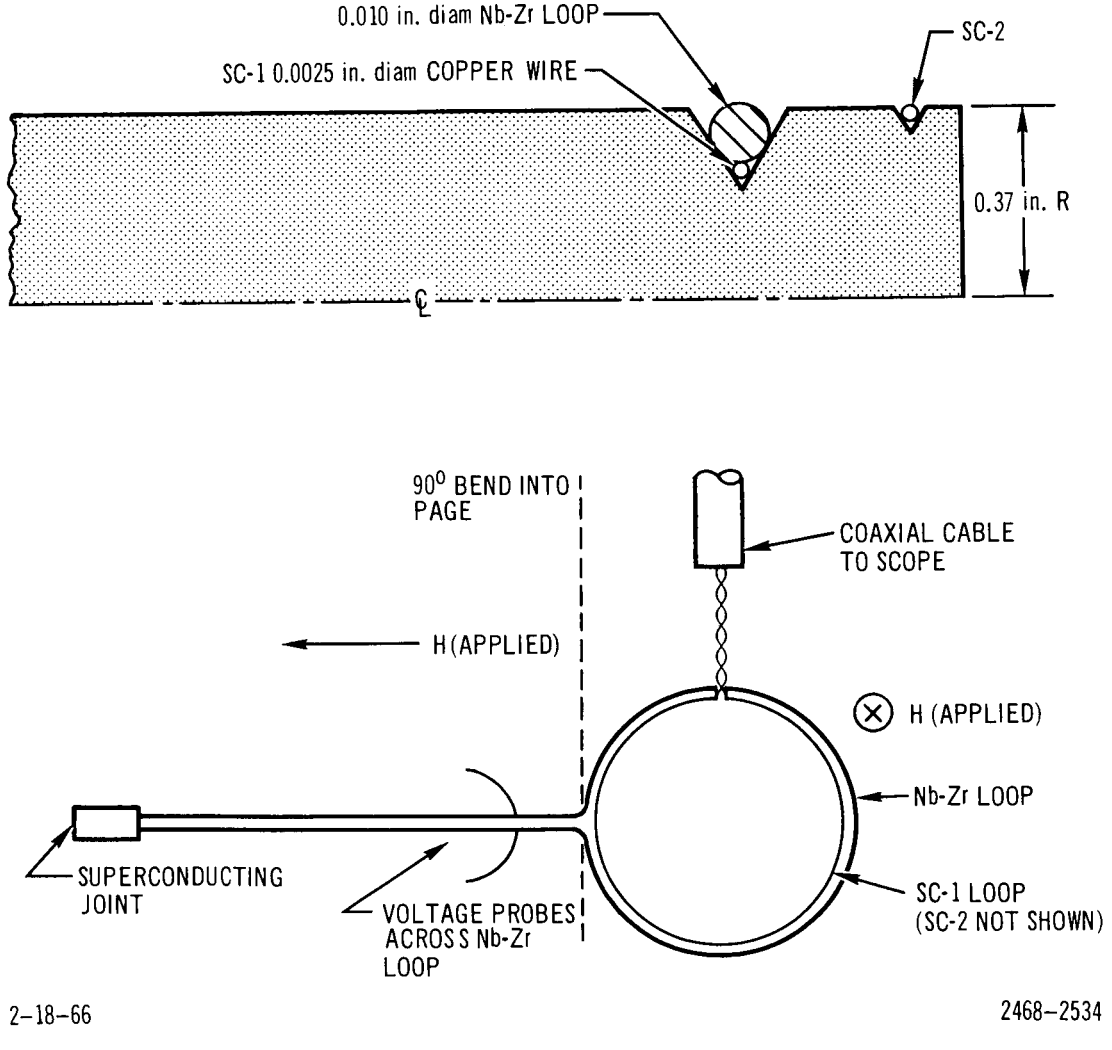

Figure 35. Sample Holders for Flux Penetration Studies

One search coil (SC-1) and the Nb-Zr wire are held in close proximity with a V groove in the Teflon holder. A second search coil (SC-2), which is removed 0.2 in. from the Nb-Zr loop, is used to monitor background noise and check for coincidences between flux jumps in the Nb-Zr loop, seen by SC-1, and the external superconducting solenoid. The ends of the Nb-Zr loop bend 90° and pass along the Teflon rod, parallel to the field, to the low-field region where a superconducting pressure joint is made. Voltage probes are attached to the Nb-Zr leads as shown. The various wires are secured with adhesive Mylar tape, and the apparatus is inserted in a 0.75-in. -ID superconducting solenoid. The Nb-Zr wire is secured between the machined V groove and the magnet coil form with a snug fit.

The two search-coils and the Nb-Zr loop voltage probes are monitored with a Tektronix Type 555 oscilloscope in conjunction with either a Tektronix Type E, high-gain plug-in unit, or a Tektronix Type 1121 preamplifier powering a Type L plug-in unit. The Type E plug-in has a sensitivity of 50 μv/cm but is limited in its frequency response, at this sensitivity, to 20 to 60 kc. The 1121 preamplifier and Type L arrangement has 15 nanosec rise-time and a sensitivity limited by the 50 μv rms noise level of the 1121 preamplifier.

The superconducting solenoid, rated at 5.00 kgauss/amp with a maximum field of 45 kgauss, is powered by an electronically controlled, regulated dc power supply. This controlled supply can deliver up to 100 amp at ramp rates of 0.001 to 10 amp/sec with a current ripple less than 10 ma.

B. EXPERIMENTS

Three separate experiments were run. In the first experiment, the superconducting loop was closed and would sustain induced persistent transport currents. The external field was increased at a rate of 200 gauss/sec. At approximately 500-gauss intervals, the loop would go normal. A typical pulse seen by the pick-up loop SC-1 is shown in Figure 36a. The trapped flux is the area under this voltage trace and equals 70 maxwells. The coupling coefficient

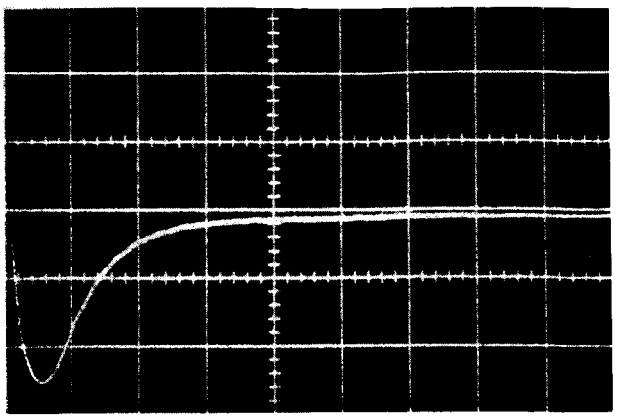

5 mv/cm

H = 15 kG

$\frac{dH}{dt}$ = 500 gauss/sec

50 μsec/cm

a. Pulse From SC-1 With Nb-Zr Loop in Persistent Mode

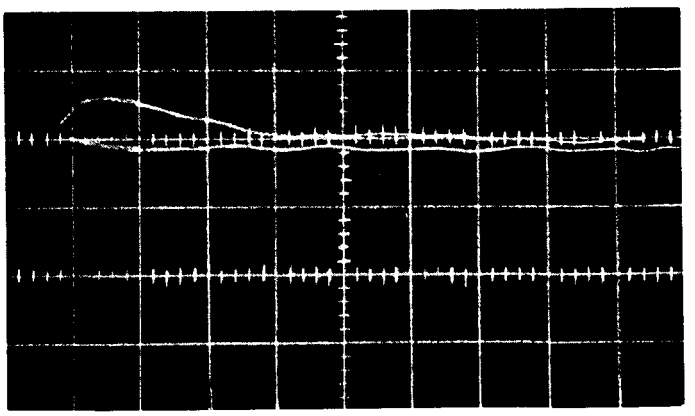

50 μv/cm

AMPLIFIER

TYPE E PLUG-IN

TEKTRONIX 1121
WITH TYPE L PLUG-IN

H = 15 kG

$\frac{dH}{dt}$ = 500 gauss/sec

UPPER TRACE: 10 μsec/cm
LOWER TRACE: 1 μsec/cm

b. Pulse From SC-1 With Nb-Zr Loop Open Circuited

2468-2514

Figure 36. Pulses From SC-1 With Nb-Zr Loop

between the Nb-Zr loop and SC-1 is calculated to be > 0.7, assuming a 0.004-in. gap between the two wires (0.001-in. insulation on each wire and an estimated 0.002-in. gap due to positioning errors). Thus, the Nb-Zr loop shielded 70/0.7 = 100 maxwells. From an IBM 7094 calculation, the flux due to a transport current in the test loop is 5.6 maxwells/amp. Thus, the current in the Nb-Zr loop is 100/5.6 = 18 amp. This value is consistent with previous findings[4] which showed that the dH/dt-induced, supercurrent instabilities in this wire (unstable Type A) began at ~20 amp. Therefore, the results of this one-turn solenoid simulation are consistent with the short-wire instability tests. (Also, see Section I. C.)

The trapped flux of ~100 maxwells is equivalent to an external field change of 280 gauss. Since SN transitions occurred for an external field change of 500 gauss, the remaining 220 gauss could result from continual field penetration while the sample is recovering from the SN transition.

It is doubtful that the loss of flux is due to flux creep as described by Kim, Hempstead, and Strnad[13, 14] because such unstable wires do not appear to permit observable flux creep during our laboratory time scale.

In the second experiment, the superconducting loop is open circuited. In this configuration, no transport current can exist in the loop, and any perturbation in the magnetic field adjacent to the wire must be due to magnetization currents in the Nb-Zr loop. If these currents reach saturation, flux penetration into the wire can occur, and pulses might be seen in SC-1.

The external field was again swept and pulses like the one recorded in Figure 36b were seen from SC-1. The upper trace was recorded using the Type E plug-in while the lower trace was recorded using the Tektronix 1121 wide-band amplifier. The lower trace is a factor of 10 faster and shows no additional character other than noise. The flux change registered is approximately 0.1 maxwells.

Coincidence observations between SC-1 and the voltage probes across the superconducting loop, see Figure 37, show that both wires see a net flux change and that this change was greater in the Nb-Zr loop. SC-2 was also monitored,

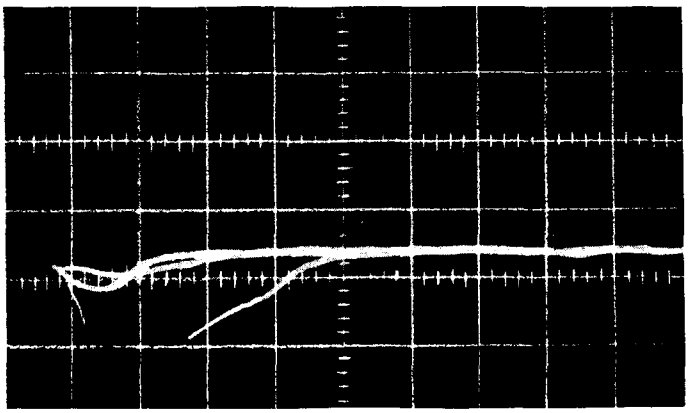

Figure 37. Simultaneous Traces From SC-1 and Nb-Zr Loop

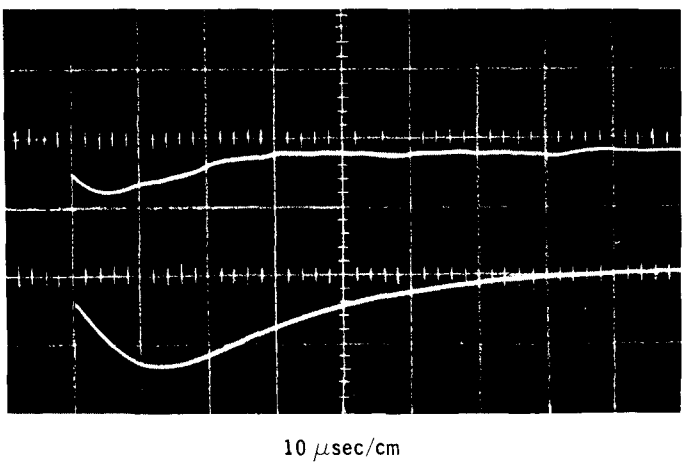

Figure 38. Pulse From 0.010-in. -Diameter Copper Wire Loop Substituting for the Nb-Zr Loop

and pulses similar to those seen from SC-1 were found but did not coincide with the SC-1 events. It appears that the pulses originated in the super-magnet but were localized.

In a third experiment, conducted to confirm the origin of these pulses, the Nb-Zr loop was replaced with a 0.010-in. -diameter copper wire. The preceding experiment was repeated and the pulses shown in Figure 38 were observed from the 0.010-in. -diameter copper wire loop. The lowest voltage trace is noise;

the intermediate trace shows typical small pulses; and the largest pulse, though partially blanked by the scope, is essentially the same as seen in the Nb-Zr loop in Figure 36a. The largest pulses were observed in the same field range (10 to 20 kG), as those seen from search coils and the Nb-Zr loop (Figures 36b and 37). Thus, the pulses observed in the second experiment originated in the windings of the supermagnet immediately adjacent to the Nb-Zr loop.

C. CONCLUSIONS

Several conclusions can be drawn from these experiments. First, critical currents in one-turn, superconducting loops parallel solenoid and short sample current behavior quite closely in that the loop critical current is essentially the same as solenoid critical currents (~18 amp) and also the same as the maximum stable super-current found in short sample tests of the same wire. Second, flux jumps could not be detected in this single turn solenoid simulation with the single loop search coils. Third, a superconducting solenoid can be a noisy source in transient magnet field work. However, supermagnets should be very quiet for constant field work, especially if persistent switches are employed.

III. MULTI-PROBE SOLENOID STUDIES

A multi-probe solenoid[4] has been tested in external fields up to 18.7 kG. The external fields, supplied by a 3-in. -ID, 8-in. -long superconducting solenoid, were homogeneous to ±10% over the volume of the multi-probe solenoid. During all tests, the external field, H_e, was held constant, while the self-field of multi-probe magnet, H_m, was increased at a constant rate of 100 gauss/sec until an SN transition occurred. The normal region was then mapped using the magnet core sensing array described in a previous report.[4] In all tests, H_e and H_m were in the same direction and were the central fields of the respective solenoid.

Figure 39 shows the multi-probe solenoid, solenoid support, and magnetic core sensing array. Figures 40a-b are cross-sectional views of the multi-probe windings and show the location and shape of the normal region after each transition. Examination of these figures reveals the following pattern. The normal region is located near one end of the solenoid when H_e = 20 kG (Figures 40a-c). At lower values of H_e (Figure 40a), the normal region is concentrated in the coil, but includes part of the central, inner windings. At still lower fields (Figure 40e), the shape of the normal region approaches that for no external field, in which the ends of the coil remain superconducting. The normal regions in Figures 40a-c are relatively small, possibly because there is less magnetic energy to propagate the normal region than in the subsequent tests.

When the multi-probe experienced an SN transition, the external solenoid would go normal also, and it is not known which coil was the initiator. No matter which coil initiated the transitions, an important result is that the transition was transferred to the second coil electromagnetically instead of thermally because in every transition the multi-probe windings between the external solenoid and the normal regions in the multi-probe coil remain superconducting.

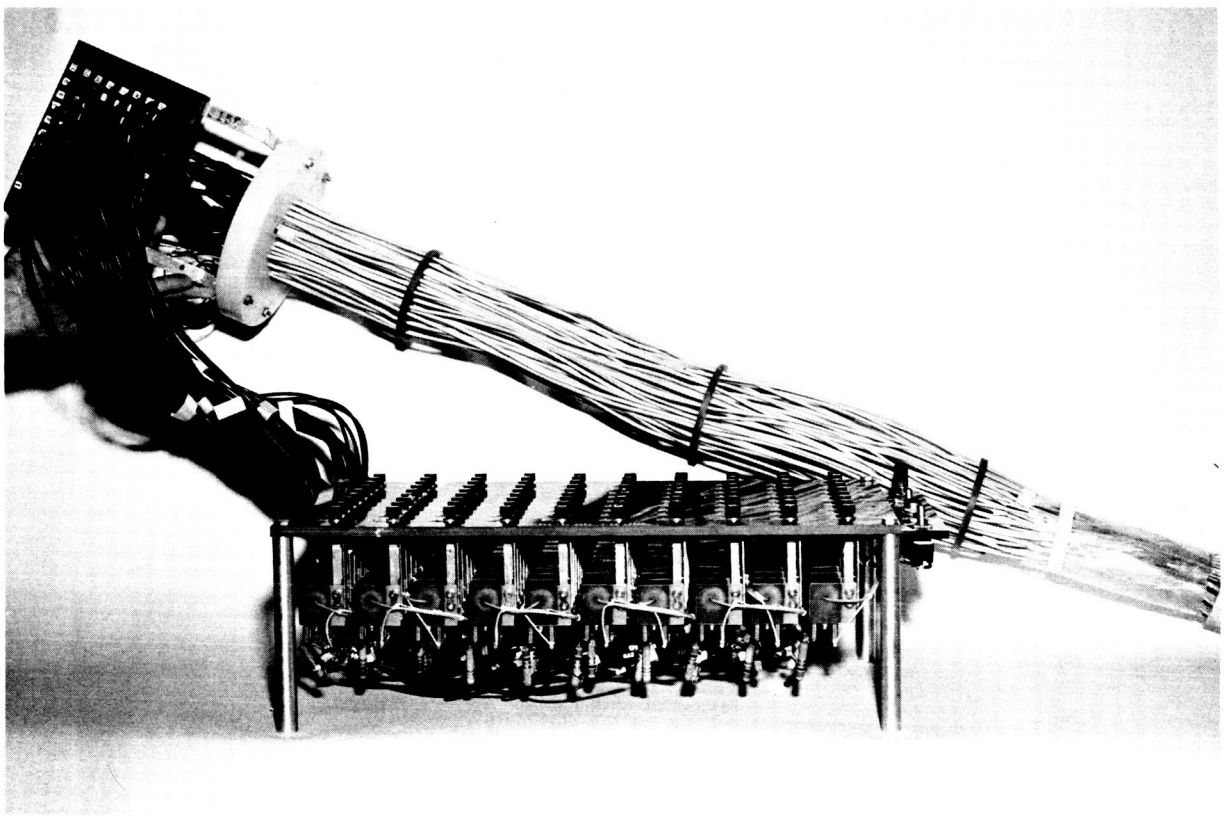

00-101329

Figure 39. Photograph of Multi-Probe Solenoid Showing Solenoid and Support Structure and 85 Pairs of Voltage Probes Leading From Solenoid to the Magnetic-Core Sensing Array

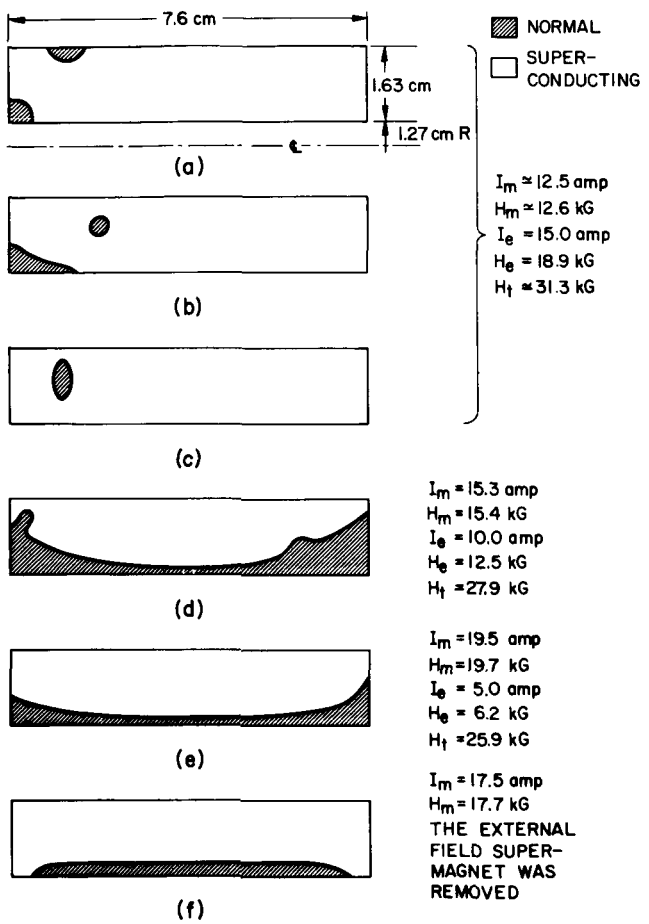

Figure 40. Multi-Probe Solenoid Cross Section Showing Super and Normal Regions After SN-Transitions in External Fields

REFERENCES

1. Berlincourt, T. G., and R. R. Hake, Phys. Rev. Letters 9, 7 (1962)

2. Vetrano, J. B., and R. W. Boom, J. Appl. Phys. 36, 1179 (1965)

3. Hansen, M., et al., Trans. Am. Inst. Mining Engrs., 191, 881-888 (1951)

4. Salter, Jr., L. C., "Summary Report - Investigation of Current Degradation Phenomenon in Superconducting Solenoids, 1963-1964," AI-64-198 (1964)

5. Lavrick, C., "Experimental Studies on the Current-Carrying Capacity of Niobium-Zirconium Wires Under Conditions of Fixed and Swept Magnetic Field," Advances in Cryogenic Engineering, 9 (1963) pp 321-7

6. Clement, J. R., and E. H. Quinnell, Rev. Sci. Instr. 23, 213 (1952)

7. Whetstone, C. N., and C. E. Roos, J. Appl. Phys. 36, 783 (1965)

8. Frank, J. P., and D. L. Martin, Can. J. Phys. 39, 1320 (1961)

9. Duwez, P., Am. Soc. Metals, 45, 934 (1953)

10. Hulm, J. K., and R. D. Blaugher, Phys. Rev. 123, 1569 (1961)

11. Clogston, A. M., Phys. Rev. Letters, 9, 266 (1962)

12. Abrikosov, A. A., J. Exptl. Theoret. Phys. (U. S. S. R.) 32, 1442 (1957)

13. Kim, Y. B., Hampstead, C. F., and Strnad, A. R., Phys. Rev. Letters 9, 306 (1962)

14. Kim, Y. B., Hampstead, C. F., and Strnad, A. R., Phys. Rev. 129, 528 (1963)